Diagenetic smectite-to-illite transition in clay-rich sediments: A reappraisal of X-ray diffraction results using the multi-specimen method

Bruno Lanson, Boris A. Sakharov, Francis Claret, Victor A. Drits

Diagenetic smectite-to-illite transition in clay-rich sediments: A reappraisal of X-ray diffraction results using the multi-specimen method

Bruno Lanson[1]
Boris A. Sakharov[2]
Francis Claret[1,3]
Victor A. Drits[2]

1 Mineralogy & Environments Group, LGCA, Maison des Géosciences, BP53, Université Joseph Fourier – CNRS, 38041 Grenoble Cedex 9, France
2 Geological Institute, Russian Academy of Sciences, 7 Pyzhevsky street, 119017 Moscow, Russia
3 BRGM, 3 av. Claude Guillemin, F-45060 Orléans cedex 2, France

*Corresponding author: bruno.lanson@obs.uf-grenoble.fr

Key words: Clay minerals, Clay diagenesis, Illite-smectite, Mixed-layering, interstratification, XRD, Gulf Coast.

ABSTRACT. Smectite illitization is a common mineralogical reaction occurring during the burial diagenesis of clay-rich sediments and shales, and has thus attracted sustained interest over the last fifty years. Prior studies have concluded that smectite illitization proceeds through a steady set of homogeneous reactions involving intermediate mixed layers of varying compositions. In these intermediate structures, illite and smectite, or, more generally, expandable layers (I and Exp layers, respectively) coexist among the same crystallites giving rise to non-periodic structures (I-Exp) characterized by specific diffraction effects. Consistent with this model, reaction progress was characterized by the simultaneous increase in the illite content in I-Exp and in their stacking order leading to the following mineralogical sequence: smectite → randomly interstratified I-Exp with high smectite contents (> 50% Exp layers) → ordered I-Exp with high illite contents (> 50% I layers) → illite. Although reaction mechanisms have been extensively debated, this structural characterization has not been challenged, possibly due to a methodological bias. In the present study, X-ray diffraction patterns typical of the diagenetic illitization of smectite are interpreted using modern approaches involving profile fitting (multi-specimen method). Novel insights into the structure of intermediate reaction products are thus obtained. In particular, original clay parageneses are described including the systematic presence of illite, kaolinite, chlorite and a mixed layer containing kaolinite and expandable layers (K-Exp).

In contrast to previous descriptions, the early stages of smectite illitization are characterized by the coexistence of discrete smectite and of a randomly interstratified I-Exp with a high content of illite layers (>50% I layers). Both the smectite and the I-Exp are authigenic and form under shallow burial, that is at low temperature conditions. With increasing burial depth, the relative proportion of I-Exp increases, essentially at the expense of discrete smectite, and the composition of I-Exp becomes slightly more

illitic. In the second stage of smectite illitization, two illite-containing mixed layers are observed. They result from two parallel reaction mechanisms affecting the randomly interstratified I-Exp present in the shallow section of the series. The first reaction implies the dissolution of this randomly interstratified I-Exp and leads to the crystallization of an ordered I-Exp without significant illitization, possibly because of the low K-availability. The second reaction affecting the randomly interstratified I-Exp implies the growth of trioctahedral (Mg, Al) hydroxide sheets in Exp interlayers, thus developing di-trioctahedral chlorite layers (Ch layers) in the initial I-Exp to form an I-Exp-Ch. A layer-by-layer mechanism is hypothesized for this reaction. In this scheme, Mg cations released by the dissolution-recrystallization reaction of I-Exp likely represent the source of Mg for the formation of brucite-like sheets in expandable interlayers, and thus of the I-Exp-Ch.

The reported structural characterization of smectite illitization intermediate products contradicts the conventional wisdom of a homogeneous reaction through a series of pure mixed layers of variable composition. In contrast, the coexistence of different phases implies a heterogeneous reaction via a sequence of intermediate phases and requires reassessing the reaction mechanisms proposed in the literature. The compositional range (relative proportion of the different layer types) of these phases is limited and smectite illitization proceeds essentially as relative proportions of the different phases vary. In addition, reaction kinetics and stability of the different intermediate products also need to be reconsidered.

INTRODUCTION

For about half a century, smectite illitization has been extensively described in different geological contexts: burial diagenesis of clay-rich sediments (Burst, 1957,1969; Weaver, 1957, 1959; Perry and Hower, 1970; Hower and others, 1976; Srodon, 1978, 1984a; Boles and Francks, 1979; Velde and others, 1986; among many others), hydrothermal alteration of volcanic tuffs (Inoue and others, 1978, 1988, 2005; Inoue and Utada, 1983; Altaner and others, 2003), metasomatic alteration of bentonites (Hoffman and Hower, 1979; Velde and Brusewitz, 1982, 1986; Inoue and others, 1990; Sucha and others, 1993; Li and others, 1997), and contact metamorphism (Nadeau and Reynolds, 1981; Pytte and Reynolds, 1989; Drits and others, 2007). Although different reaction mechanisms have been inferred (see Altaner and Ylagan, 1997, for a review; Srodon and others, 2000), this mineralogical transition has been systematically described to occur through mixed layers. In these intermediate structures, illite and smectite, or more generally expandable, layers (I and Exp layers, respectively) coexist among the same crystallites giving rise to non-periodic structures, hereafter referred to as I-Exp. The structural characterization of I-Exp, essential for the reconstruction of thermal and chemical paleoconditions, requires determining the nature of interstratified layers, their relative proportions and their stacking sequences through analysis of their specific diffraction effects (see Reynolds, 1980, Drits and Tchoubar, 1990, Moore and Reynolds, 1997, for details). Such analysis has revealed that smectite illitization is a continuous two-stage reaction characterized by a steady increase of the illite content in I-Exp and by the simultaneous increase of stacking order: illite and expandable layers are interstratified at random when expandable layers dominate ("R0 zone" – early diagenesis), whereas interstratification is ordered when illite prevails ("R $\geq$ 1 zone" – late-stage diagenesis; Shutov and others, 1969;

89 Perry and Hower, 1970, 1972; Hower and others, 1976; Bethke and others, 1986; Srodon,
90 1999).

91 Following these pioneering works, simplified methods have been proposed for the
92 structural characterization of I-Exp from X-ray diffraction (XRD) data (Srodon, 1980, 1981,
93 1984b; Watanabe, 1981, 1988; Velde and others, 1986; Inoue and others, 1989; Moore and
94 Reynolds, 1997). These methods essentially rely on peak migration curves which link the
95 position of a given reflection (or of a set of reflections) to the composition (relative proportion
96 of the different layer types) of the mixed layers and to their stacking order. Peak migration
97 curves were obtained mostly from XRD patterns calculated using programs implemented
98 from Reynolds (1967, 1980) or Watanabe (1981) algorithms. These calculations were
99 essentially restricted to I-Exp composition and ordering that were described in the early works
100 reported above, thus confining the simplified identification methods to these specific mixed
101 layers. Logically, the early description of smectite illitization was not challenged by the
102 numerous subsequent case studies. The lack of direct comparison between experimental and
103 calculated XRD patterns concealed possible incomplete or erroneous identifications. A
104 significant proportion of the studies devoted to smectite illitization thus focused on the
105 definition of reaction mechanisms and on the possible use of this mineralogical
106 transformation as a paleogeothermometer. For the latter purpose, the influence of time and
107 temperature (Hower and others, 1976; Velde and Vasseur, 1992), K availability (Huang,
108 1993; Bauer and Velde, 1999), and water/rock ratio (Whitney, 1990) on reaction progress was
109 estimated.

110 However, a more appropriate crystallography-based approach has been developed over
111 the last decade. In particular, direct comparison between calculated and experimental
112 diffraction patterns has been favored and has allowed reproduction of not only the positions of
113 the reflections but also of their profiles, both of which are strongly influenced by

interstratification. In addition to the frequent occurrence of multi-component mixed layers in nature, the multi-specimen method proposed initially by Drits and others (1997), and by Sakharov and others (1999a, 1999b) uncovered the existence of mixed layers exhibiting "unusual" composition and/or stacking order (Drits and others, 1997, 2002a, 2002b, 2004, 2007; Sakharov and others, 1999b, 2004; Lindgreen and others, 2000, 2002; Claret and others, 2004; McCarty and others, 2004). This new approach thus challenges the commonly accepted description of smectite illitization in diagenetic series by invalidating hypotheses sustaining usual I-Exp identification criteria such as homogeneity of the swelling behavior, random interstratification restricted to smectite-dominated mixed layers, absence of segregation and of partial ordering, et cetera (see Lanson, 2005, for further discussion).

The present study thus aims at obtaining an accurate structural characterization of samples characteristic of diagenetic smectite illitization in clay-rich sediments from modeling of their XRD patterns. The proposed models are shown to be consistent with the coexistence of discrete smectite with I-Exp, as has been observed on similar samples with transmission electron microscopy. In addition, the definition of structure models at various stages of the reaction constrains the possible reaction mechanisms of this transformation. In particular, analysis of stacking parameters refutes the solid-state transformation hypothesis for illitization of I-Exp over the "R0 zone", and for the transition from randomly interstratified I-Exp to ordered varieties, consistent with crystal growth features reported during smectite illitization. It is shown also that part of the I-Exp formed early in the "R0 zone" transforms, possibly through solid-state processes, into a complex mixed layer present in the deeper samples.

MATERIALS AND METHODS

Samples

Samples were collected in two different onshore wells in the Texas Gulf Coast (Carter – Tyler County in central Gulf Coast Texas, and Mustang Island – Nueces County in south Gulf Coast Texas). These wells have been described previously by Velde and Espitalié (1989), and Velde and Vasseur (1992), and the stratigraphic age of the samples ranges from Cretaceous to Eocene (Carter well) and from Eocene to Pleistocene (Mustang Island). In the two wells, little or no erosion has occurred and present depths are approximately maximum burial depths. The temperature gradient is similar in both wells (32.7°C/km and 35°C/km, in Mustang Island and Carter, respectively), and they both extend through most of the smectite-to-illite transition (fig. 1).

Experimental

Carbonates were removed from all samples using the acetic acid-acetate buffer method described in Moore and Reynolds (1997). Then, organic matter was removed at 50°C by adding small aliquots of hydrogen peroxide (H_2O_2 – 30%) to the suspension until gaseous emission ceased. The <2 μm size fraction was extracted by centrifugation for a set of samples selected from -2170 to -5500 m in Carter and Mustang Island boreholes. From preliminary XRD results, 6 of the initial samples were selected as representative of the complete transition between "smectite-rich" and "illite-rich" samples in Gulf Coast series. All samples were selected in the Carter well at 2170, 3660, 4000, 4640, 5010, and 5180 m (samples A-F).

To minimize the contributions from mica, kaolinite, chlorite and quartz, the <0.2 μm size fraction was extracted for these 6 samples. This fraction was then Ca-saturated. Suspensions were kept in contact with a 1M $CaCl_2$ solution for 4-12 hours at room

161 temperature to ensure a complete cation exchange. After three replications of this procedure,
162 the excess chloride was rinsed with distilled water (Milli-Q – 18.2 MΩ.cm^{-1}).
163 Oriented preparations were obtained by pipetting a slurry of the Ca-saturated
164 suspensions on a glass side and drying this suspension at 40°C for a few hours to obtain an
165 air-dried (AD) preparation. Ethylene-glycol (EG) solvation of the slides was achieved by
166 exposing them to EG vapor at 70°C for a minimum of 12 hours. XRD patterns were recorded
167 with a Bruker D5000 powder diffractometer equipped with a Kevex Si(Li) solid state detector
168 using CuKα_{1+2} radiation. Intensities were recorded at 0.04° 2θ step intervals from 2 to 50°,
169 using a 6 sec counting time per step except for sample D (40 sec/step). Sizes of the divergence
170 slit, the two Soller slits, the antiscatter, and resolution slits were 0.5°, 2.3°, 2.3°, 0.5° and
171 0.06°, respectively. Humidity was controlled at 40% RH for AD measurements.
172
173 *XRD Profile Modeling*
174 Structure models were determined using the multi-specimen method described by Drits
175 and others (1997), and Sakharov and others (1999a, 1999b). In contrast to usual identification
176 methods of mixed layers, the multi-specimen method requires recording XRD patterns after
177 different treatments for each sample. For a given sample, these patterns usually differ
178 significantly because of the contrasting hydration/expansion behavior of expandable
179 interlayers in response to these treatments. The method itself relies on the direct comparison
180 of experimental profiles with those calculated for a structure model, the optimum agreement
181 between data and calculated patterns being obtained by a trial-and-error procedure.
182 The different treatments can affect the thickness and scattering power (nature, amount,
183 and position of interlayer species) of the expandable interlayers, but not the layer sequences
184 within the crystallites. As a consequence, a consistent structure model is obtained for a given
185 mixed layer when layer sequences obtained from all experimental profiles of a given sample

186 are nearly identical. XRD pattern modeling provides also a quantitative phase analysis of the
187 samples. One essential requirement for structure model soundness is that the relative weight
188 contributions of periodic and interstratified phases to the different XRD patterns of a given
189 sample must be similar (Sakharov and others, 1999b; Claret, 2001; Lindgreen and others,
190 2002; McCarty and others, 2004, 2005).

191 Structure models for each mixed layer include the number of the different layer types
192 (not limited to 2), their nature and relative proportions. Markovian statistics are used to
193 describe possible layer stacking sequences and the relative abundance thereof. An important
194 parameter of this statistical description is the Reichweit parameter R (Jagodzinski, 1949)
195 which characterizes the extent of ordering as the number of adjacent layers influencing the
196 nature of a given layer. For R = 0, layer types are thus randomly interstratified, whereas for
197 R = 1 the occurrence probability of a given layer type depends on the nature of its nearest
198 predecessor. For a given value of the R parameter, a set of probability parameters is needed to
199 completely describe layer stacking. The relative content of the different layer types (W_i) is
200 systematically needed together with junction probability parameters (P_{ij}). P_{ij} parameters
201 define the probability for a j-type layer to follow an i-type layer (i,j = I or Exp for I-Exp). W_i
202 and P_{ij} parameters are related, and only two parameters are necessary to describe a two-
203 component mixed layer with R = 1, W_I and P_{ExpExp} being commonly used for I-Exp. In this
204 case, specific layer stacking modes for R = 1 include maximum possible degree of ordering
205 (MPDO), which is obtained when pairs of the least abundant layers are prohibited in the
206 stacking, that is when $P_{ExpExp} = 0$ assuming $W_I > W_{Exp}$. Random interstratification occurs
207 when $P_{ExpExp} = P_{IExp} = W_{Exp} = 1 - W_I$, and physical mixture of I and Exp layers when P_{ExpExp} =
208 1 whatever the W_{Exp} value. In addition, a tendency to segregation of i-type layers is
209 characterized by $W_i < P_{ii}$ (i = I, Exp), whereas partial ordering occurs when $W_{Exp} > P_{ExpExp} > 0$

assuming $W_I > W_{Exp}$ (see Bethke and Altaner, 1986, Drits and Tchoubar, 1990, and Moore and Reynolds, 1997, for details).

The algorithm developed initially by Drits and Sakharov (1976) and used recently by Drits and others (1997) and Sakharov and others (1999b) was used to fit experimental XRD profiles over the 2–50° 2θ range. Instrumental and experimental factors such as horizontal and vertical beam divergences, goniometer radius, length and thickness of the oriented slides were measured and introduced without further adjustment. Sigmastar (see Reynolds, 1986, for details) was set to 12 and the mass absorption coefficient (μ^*) to 45, as recommended by Moore and Reynolds (1997). In the profile fitting process, it was necessary to define different types of Exp layers as a function of their hydration or swelling behavior in AD and EG states, respectively (Drits and others, 2002a). Irrespective of the hydration/swelling behavior of Exp layers, the relative contents of I and Exp layers and their stacking sequences should be the same in both AD and EG states. The hydration/swelling behavior of Exp layers is likely related to the amount and location of the layer charge deficit, although this behavior may differ for a given layer from AD to EG states. In the following I, K, Ch, and Exp denote illite, kaolinite, di-trioctahedral chlorite, and expandable layers, respectively. For all layer types *z* atomic coordinates proposed by Moore and Reynolds (1997) were used after modification to fit the layer thickness values used for simulation; thermal motion parameters (B) were also set as proposed by Moore and Reynolds (1997). The position and amount of interlayer species (H_2O and EG molecules in particular) were considered as variable parameters and varied about the values proposed by Moore and Reynolds (1997) during the fitting process. In bi-hydrated Exp layers (2W), a single plane of H_2O molecules was assumed to be present on each side of the interlayer mid-plane as proposed by Ferrage and others (2005a, 2005b).

Finally, distributions of coherent scattering domain sizes (CSDSs) were assumed to be lognormal and characterized by their mean value (Drits and others, 1997b). Quality of fit was

assessed over the 4-50°2θ (22.0-1.85 Å) range with the R_{wp} and R_{exp} factors (Howard and Preston, 1989).

RESULTS

Qualitative Description of the Experimental XRD Patterns.

Evolution of sample structure with depth is best seen on XRD patterns obtained after EG solvation (fig. 2A). The XRD pattern of sample A (2170 m) exhibits a strong peak at ~16.9 Å, well resolved on its low-angle side, and weaker peaks at 8.6, 5.54, 3.331, 2.781, and 2.023 Å that form a non-rational series. In addition, peaks at 7.21, 3.58 and 2.38 Å and weak modulations at ~10.0 and 5.0 Å correspond to finely dispersed kaolinite and to discrete illite, respectively. The peak at ~17.0 Å is still intense for sample B (3660 m) but its resolution is significantly reduced on its low-angle side. Compared to sample A, the reflections at 5.54 Å and 2.781 Å are shifted to higher and lower angles, respectively, in the XRD pattern of sample B. The reflection at 8.6 Å (sample A) is shifted also to lower angles and appears as a high-angle shoulder of the 10.0 Å reflection (sample B). XRD patterns of samples B and C are alike, except that the low-angle resolution of the ~17.0 Å peak is reduced for sample C compared to sample B. Samples B and C also contain significant amounts of discrete illite and kaolinite, and a small amount of chlorite.

XRD patterns of samples taken from depths > 4500 m (D, E, and F) are all akin and their profiles strongly differ from those of samples A, B and C. Over the low-angle region, there is no peak at ~17.0 Å, but broad maxima between ~13.5-15.0 Å (fig. 2). These patterns also contain a super-reflection at ~30 Å, best seen for sample E, and additional broad maxima at ~9.25-9.30 Å, and 5.20-5.25 Å. The low resolution of the latter reflections results to some

extent from their partial overlap with illite peaks at 10.0 Å and 5.0 Å. Finally, sharp kaolinite and chlorite reflections are visible at 3.579 Å and 3.528 Å.

To summarize the above observations, the six samples can be divided in two groups. XRD patterns of group I (samples A, B, and C) exhibit a ~17.0 Å reflection (EG state) whose low-angle resolution decreases with increasing depth. XRD patterns of group II (samples D, E, and F) exhibit a broad maximum at ~13.5-15.0 Å and a super-reflection at ~30 Å. XRD patterns collected in AD conditions are shown in the Appendix (fig. A-1).

The described evolution of XRD patterns with depth is typical for smectite illitization resulting from the burial diagenesis of clay-rich rocks. For example, XRD patterns presented by Perry and Hower (1970) for samples E-2131 m, E-2554 m, and E-2667 m are almost superimposed (except for the kaolinite reflections) to those of samples A, B and C, respectively (fig. 3). Similarly, the XRD pattern presented by Perry and Hower (1970) for sample E-3658 m resembles that of samples D and E, except for the low-angle intensity. According to Hower and others (1976) the observed evolution is evidence for a continuous smectite-to-illite reaction series occurring through intermediate mixed layers. However in both the Perry and Hower (1970) and Hower and others (1976) studies, XRD pattern interpretation was restricted to a qualitative comparison with patterns calculated for two-component I-Exp (EG) models. The relative proportions of I and Exp layer types (W_i), and their ordering (P_{ij} parameters) were the two essential parameters refined.

Quantitative Description of Experimental XRD Profiles

Group I samples: single-phase segregated I-Exp model.– According to this model, the non-rational series of basal reflections corresponds to a unique I-Exp in which I and Exp layers tend to segregate. XRD data are compared to calculated patterns in figure 4. Structural parameters used to calculate these patterns are listed in tables 1 and 2. Along with the main I-

Exp contribution, samples contain kaolinite, illite (an illite-rich mixed layer with ~ 5% of expandable layers), minor chlorite, and a randomly interstratified K-Exp containing 75% kaolinite and 25% expandable layers. Although K-Exp have attracted considerably less attention than I-Exp, natural K-Exp covering the whole compositional range have been reported in the literature (see for example Sakharov and Drits, 1973; Sudo and Shimoda, 1977; Brindley and others, 1983). Consistent with these reports, K-Exp whose composition is dominated by kaolinite layers exhibit broad diffraction maxima shifted from the ideal kaolinite maxima towards the nearest smectite peaks as predicted by Méring (1949).

Transition from sample A to sample C corresponds to an increase in illite and K-Exp content (from 5 to ~21%, and from 5 to ~15%, respectively – table 2) and to a decrease of I-Exp (from 79 to ~53%). The kaolinite and chlorite content is about constant. With increasing depth, I-Exp expandability decreases from 55% in sample A to 35% in samples B and C (table 1A). Under AD conditions, three types of expandable layers (15.0, 12.5 and 14.0 Å layers) are found in I-Exp from sample A, whereas only 2W and 1W layers (15.0 and 12.5 Å, respectively) are encountered in samples B and C. After EG solvation all Exp layers in I-Exp from sample A swell to 16.76 Å with two planes of EG molecules in their interlayers (2EG layers). Swelling behavior is more heterogeneous in samples B and C (table 1A). In all three samples, $W_I < P_{II}$ (table 1B) for I-Exp and illite layers are thus slightly segregated, as estimated by the S_q parameter (Drits and Tchoubar, 1990):

$$S_q = (P_{ii} - W_i)/(1 - W_i) \quad (1)$$

To determine S_q, it is convenient to use P_{II} and W_I values so as to disregard the actual distribution of Exp layers. With increasing depth, the S_q parameter decreases from 0.27 to 0.19 and 0.10 (samples A, B and C, respectively), indicating that interstratification of I and

309 Exp layers tends to become random with increasing burial depth and illite content (table 1A).
310 The CSDS of I-Exp increases with burial depth from 7 (sample A) to 15 layers (samples B
311 and C – table 1A). For a given sample, the P_{ij} parameters refined for the I-Exp are different
312 for AD and EG states (table 1B). This apparent inconsistency arises from the contrasting
313 expansion behavior of Exp layers in AD and EG states, and vanishes if the hydration/swelling
314 behavior of Exp layers is carefully analyzed (see Appendix for details).
315 *Single-phase segregated I-Exp model: Intrinsic inconsistency of the model.*– If I-Exp in
316 group I samples represent a series of diagenetically altered mixed layers, the occurrence
317 probabilities of I and Exp layers, and those of the different layer pairs and triplets (W_i, W_{ij} =
318 $W_i \times P_{ij}$ and $W_{ijk} = W_i \times P_{ij} \times P_{jk}$, respectively – table 3) should evolve logically in the context
319 of illitization. For the sake of simplicity, all expandable layers will be considered together in
320 the following discussion. From these occurrence probabilities, transition from sample A to
321 sample B appears logical as the illite enrichment (from 45% to 65% at 2170 and 3660 m,
322 respectively) is associated with the decrease of occurrence probability for layer pairs, and
323 layer triplets (not shown), containing Exp layers (table 3). At the same time, the segregation
324 degree in I-Exp decreases from 0.27 (sample A) to 0.19 (sample B) because ExpExp pairs
325 disappear faster than II pairs form [$(W_{ExpExp})_B - (W_{ExpExp})_A = -0.205$, and $(W_{II})_B - (W_{II})_A =$
326 0.194 – table 3].
327 In the general illitization scheme, the steady evolution of a segregated I-Exp towards
328 random interstratification is a priori consistent with a solid-state transformation. The observed
329 decrease of the S_q parameter between samples B (0.19) and C (0.10) follows the same logic
330 although illite contents are similar in the two samples (table 3). However, when looking at the
331 different W_{ij} probabilities, the I-Exp evolution between samples B and C cannot be
332 interpreted reasonably in the illitization context. This evolution implies indeed the formation
333 of IExp and ExpI pairs at the expense of both II and ExpExp pairs [$(W_{II})_B > (W_{II})_C$ – table 3].

334 The single-phase segregated I-Exp model is thus inadequate to describe the structural
335 evolution of group I samples, and should be rejected.
336 *Group I samples: The mixture model.*– According to this model, the ~17 Å peak of
337 group I samples corresponds to discrete smectite coexisting with a randomly interstratified I-
338 Exp with a high content of illite layers (W_I > 50% – Claret, 2001; Drits and others, 2002b;
339 Claret and others, 2004; Lanson and others, 2005; McCarty, 2005; Aplin and others, 2006;
340 McCarty and others, 2008). Data are compared in figure 5 to XRD patterns calculated for this
341 model. Table 4A contains the structural and probability parameters for the I-Exp contribution,
342 whereas relative proportions of the different contributions to the diffraction patterns are
343 reported in table 5. In all group I samples, the major contribution is I-Exp whose relative
344 proportion increases with increasing burial depth from 44% to 50% and 57% (samples A, B
345 and C, respectively). Simultaneously, the content of discrete smectite decreases dramatically
346 from 27% to 5% and ~2% in samples A, B and C, respectively. As for the single-phase
347 segregated I-Exp model the content of discrete illite increases significantly with depth from
348 5% to ~17% and 21% in samples A, B and C. I-Exp is randomly interstratified despite its high
349 illite content that ranges from 57% to 62 and 67% (samples A, B and C, respectively). I-Exp
350 has the same mean (12 layers) and maximum (50 layers) CSDS in all group I samples (table
351 4A). A randomly interstratified K-Exp with 75% kaolinite layers completes the clay
352 paragenesis. K-Exp exhibits broad diffraction maxima at ~6.8-7.0 and 3.4-3.5 Å both in AD
353 state and after EG solvation (fig. A-2A, B).
354 *Group II samples.*– Along with 4-5% of chlorite, 5-10% of illite (with 5% Exp layers),
355 6-12% of kaolinite, all group II samples contain I-Exp, I-Exp-Ch and K-Exp mixed layers.
356 The structural and probability parameters providing the best fit to XRD data (fig. 5) are
357 reported in table 4C. The major phases are I-Exp and I-Exp-Ch. The relative proportion of I-
358 Exp decreases slightly with burial depth from 40% (sample D) to 33 and 34% (samples E and

F, respectively) whereas that of I-Exp-Ch steadily increases from 27% to 31% and 42% (samples D, E and F, respectively).

Parallel to this phase composition change, transition from sample D to sample F is characterized by a slight increase of the illite content in I-Exp (from 70 to 75%). In sample D, interstratification of I and Exp layers is ordered (R = 1) with MPDO ($P_{Exp1Exp1} = P_{Exp1Exp2} = P_{Exp2Exp1} = P_{Exp2Exp2} = 0$). Longer-range ordering (R = 2 – table 4C) is observed for samples E and F. In the latter samples P_{ij} parameters are similar to sample D, and longer-range ordering is characterized by a slight segregation of IExpIExp sequences as $P_{ExpIExp} > W_{Exp} / W_I$ (see Drits and Tchoubar, 1990, for details). Compared to I-Exp in group I samples, the size of I-Exp CSDs is significantly increased for group II samples (mean and maximum values are 15 and 100 layers compared to 12 and 50, respectively, for group I samples – tables 4A, 4C). In all group II samples, I-Exp-Ch contains 70% of illite layers interstratified with Exp and di-trioctahedral chlorite layers, the proportion of Ch layers increasing from 15% in samples D and E, to 20% in sample F. In contrast to the ordered I-Exp, I-Exp-Ch CSDSs are similar to those determined for the I-Exp in group I samples (tables 4A, 4C). Finally, K-Exp (R = 0) consists of 75% kaolinite and 25% Exp layers as in group I samples.

DISCUSSION

Reliability of Structure Models

The results obtained in the present work demonstrate the ability of the multi-specimen approach to provide good quality fit to experimental data obtained on natural polyphasic samples, in agreement with previous studies (Drits and others, 1997a, 2002a, 2002b, 2004; Sakharov and others, 1999a, 1999b; Lindgreen and others, 2000, 2002; Claret and others, 2004; McCarty and others, 2004, 2008). This approach can thus be used to determine accurate

structural parameters for the phases present in a given sample. In the present work, satisfactory fit to experimental positions, intensities and profiles of basal XRD reflections was obtained using up to three mixed layers, each incorporating from two to four layer types, in addition to discrete phases.

Obviously, the more discrete and mixed-layer phases that coexist in a sample, the more independent structural parameters that are needed for simulation. As a result, the reliability and accuracy in determining these parameters may decrease as more phases are introduced, although constraints are provided by the required uniqueness of structure models used to fit different patterns of a given sample (AD and EG patterns of Ca-saturated samples in the present case).

Evidence for the actual phase composition.– As the optimum fits to XRD data were obtained using a trial-and-error approach, the actual sensitivity of XRD simulations to key structural parameters needs to be assessed. The presence of the different contributions is the first of these parameters, and samples B and E will be used as typical for group I and II, respectively. Elementary contributions to the intensity diffracted by these two samples are shown in the Appendix (fig. A-2, A-3). Figure 6 compares the XRD pattern of sample B with those calculated for models similar to the optimal one (fig. 5) after subtraction of the contributions of discrete smectite or of K-Exp. Logically, the absence of the minor smectite contribution leads to the absence of the 17 Å peak in the calculated EG pattern (fig. 6A – R_{wp} = 17.56%). Similarly, the absence of the K-Exp contribution leads to significant misfits at ~11.5^{o} and ~26^{o}2θ (fig. 6B – R_{wp} = 16.00%).

For group II samples, exclusion of either I-Exp or I-Exp-Ch contributions in the calculated XRD pattern decreases dramatically the agreement with the data. For example, calculated intensity is reduced in the low-angle region if the I-Exp contribution is subtracted from the optimal fit (fig. 7A). Additional significant misfits are observed at 16-19^{o} 2θ and 26-

409 36^{o} 2θ in both EG and AD XRD patterns (fig. 7A – R_{wp} = 23.04%, and fig. 7B – R_{wp} =
410 27.73%, respectively). Figure 7C (R_{wp} = 20.62%) shows that the I-Exp-Ch contribution is
411 essential to fit the AD pattern in the 18-20 and 26-31^{o} 2θ ranges. In the present work, mixed
412 layers are introduced only if they allowed fitting specific angular ranges without significant
413 overlap with other phases.

414 *Evidence for the presence of chlorite layers in I-Exp-Ch.*– The actual nature of the
415 mixed layer coexisting with the ordered I-Exp was determined after testing numerous illite-
416 containing structure models with contrasting amounts, and distributions, of Exp layers: in
417 addition to I and Exp layers the optimum mixed layer (I-Exp-Ch) contains di-trioctahedral
418 layers consisting of dioctahedral 2:1 layers and of trioctahedral brucite-like interlayer sheets.
419 Despite a similar basal spacing, the 14.0 Å Ch layers can be differentiated from 14.0 Å Exp
420 layers because of their contrasting scattering factors. If Ch layers (with 3.0 Mg and 6.0 OH
421 per half unit-cell in their interlayers) are replaced by Exp layers (with 0.25 Mg and 2.0 H_2O
422 per half unit-cell in their interlayers), significant misfits are visible at 17-18^{o} and 26-31^{o} 2θ
423 for sample E (fig. 8A – R_{wp} = 17.41%). XRD patterns calculated for the optimum I-Exp-Ch
424 contribution and for the contribution in which Ch layers are replaced by Exp layers are shown
425 in figure A-4. The strong intensity increase at 17-18^{o} 2θ induced by the presence of Ch layers
426 is related to the specific intensity distribution observed for sudoite (di-trioctahedral chlorite),
427 whose 4.7 Å reflection is most intense (Lin and Bailey, 1985; Billault and others, 2002;
428 Kameda and others, 2007).

429 *Heterogeneous hydration/swelling of Exp layers.*– In both AD and EG states, Exp layers
430 present in mixed layers often exhibit various interlayer configurations and *d*-spacings as
431 reported for reference smectite samples (Ferrage and others, 2005b, 2007). For example, in
432 the AD state I-Exp from group I samples systematically contains 15.0, 14.0 and 12.5 Å layers
433 (table 4). Sensitivity of XRD to such heterogeneous behavior may be assessed by replacing,

434 for example, 14.0 Å Exp layers (8% of the layers in I-Exp from sample B) either by 15.0 Å or
435 by 12.5 Å layers (fig. 8B and C, respectively). In both cases, significant misfits are visible at
436 28-30^{o} 2θ.
437
438 *Diagenetic Illitization of Clay-rich Sediments: A Two-Stage Process*
439 Undoubtedly, illitization of clay-rich sediments during burial diagenesis of mudstones
440 and shales ranks among the most important and most documented mineral reactions. In the
441 present work, the innovative interpretation of XRD patterns provides detailed information on
442 the different phases present in the sediments and on their evolution. As a result, a structural
443 mechanism can be proposed which contrasts with the usual description of a continuous
444 transformation described by Perry and Hower (1970), Hower and others (1976) and many
445 other authors (see Srodon, 1999, for a review). According to this commonly accepted model,
446 diagenetic illitization of clay-rich sediments consists of two main stages whose existence is
447 not challenged in the present study. The evolution of the mineralogical composition, and the
448 structural evolution of individual phases will thus be described separately for group I and
449 group II samples.
450 *Smectite illitization in the upper part of the series (group I samples).*– The commonly
451 accepted model assumes the steady illitization of a unique randomly interstratified I-Exp. By
452 contrast two phases, a discrete smectite and a randomly interstratified I-Exp with high illite
453 content, coexist in group I samples in addition to discrete illite, kaolinite, K-Exp and chlorite
454 (except for sample A). When burial depth increases the relative proportion of discrete
455 smectite decreases sharply from 27% at 2170 m to 2-3% at 4000 m and the illite content in I-
456 Exp increases (from 57% to 67% at the same depths). Except for a few early reports (Perry
457 and Hower, 1970, 1972; Reynolds and Hower, 1970; Bethke and others, 1986), randomly
458 interstratified I-Exp with such high illite contents have seldom been described in diagenetic

459 environments, interstratification of I and Exp layers being usually described as ordered (R = 1
460 and MPDO) when illite layers prevail. However, the coexistence of discrete smectite with
461 randomly interstratified I-Exp with high illite content is possibly widespread at shallow depth
462 in sedimentary basins, the absence of significant maximum in the low-angle region being
463 responsible for their scarce description. The steady decrease of the 17.0 Å peak intensity and
464 of its low-angle resolution observed with depth for group I samples is indeed characteristic of
465 the early stage of the diagenetic smectite-to-illite transition (fig. 3).
466 A similar mineralogical composition was described in the Callovo-Oxfordian
467 sedimentary formation (Paris Basin – Claret, 2001; Claret and others, 2004). Using the same
468 methodological approach McCarty (2005), and McCarty and others (2008) also demonstrated
469 that discrete smectite and randomly interstratified I-Exp with high illite content coexist in
470 shallow samples from the off-shore Gulf Coast. The similarities between the XRD patterns
471 recorded for group I samples and those obtained from Gulf Coast wells B and E by Perry and
472 Hower (1970, 1972) support such a coexistence in the latter samples. TEM observations
473 performed on shallow samples from various sedimentary basins also support the ubiquity of
474 such a clay paragenesis (Dong and others, 1997; Dong, 2005; Freed and Peacor, 1992).
475 I-Exp in group I samples are characterized also by heterogeneous hydration/swelling
476 behavior of Exp layers. In the AD state, 1W (d_{001} ~ 12.5 Å) and 2W (d_{001} ~ 15.0 Å) layers
477 systematically coexist in I-Exp (table 4), most likely as a consequence of the heterogeneous
478 distribution of the amount and/or location of the layer-charge deficit. However, layer-charge
479 heterogeneity is likely not considerable as both layer types swell to 16.7-16.9 Å following EG
480 solvation (table 4). In addition, I-Exp includes 14.0 Å layers present in similar proportions
481 under AD and EG conditions. These layers cannot be considered as smectite layers as their
482 basal spacing remains constant upon EG solvation, and their actual nature is unclear. Their
483 basal spacing and swelling behavior are consistent with hydroxy-interlayered vermiculite

484 layers that are often found in soils as a separate phase (Douglas, 1989; Moore and Reynolds,
485 1997; Chen and others, 2001; Marques and others, 2002). The observed hydration/swelling
486 heterogeneity of Exp layers is most likely common in natural samples, thus impairing the
487 potential of most usual identification methods for I-Exp as discussed in more detail by
488 McCarty and others (2008).
489 *Group I samples: origin of the randomly interstratified I-Exp with high illite content*
490 *(~65%I).*– It is commonly assumed that the smectite-to-illite reaction starts from a pure
491 smectite precursor. However, Hower and others (1976) pointed out that in young sedimentary
492 basins the pure smectite stage may be concealed by the high variability of smectite contents in
493 randomly interstratified I-Exp from surface samples. According to Jennings and Thompson
494 (1986) and Velde and Vasseur (1992), the compositional homogenization of I-Exp, likely
495 through its recrystallization and formation of pure smectite, occurs at burial depths ranging
496 typically from several hundred meters in older rocks to 1-2 km in younger ones. Smectite then
497 acts as a precursor for the diagenetic smectite-to-illite conversion (Velde and Iijima, 1988). In
498 the Carter well, the presence of pure smectite was inferred at 683 m from XRD analysis
499 (Berger and others, 1999). In the present study, no XRD data were collected over the 683-
500 2150 m depth interval. It is however reasonable to assume that steady smectite-to-illite
501 conversion occurs over this depth interval, and that both smectite and I-Exp are authigenic in
502 group I samples. Additional support for the authigenic origin of I-Exp comes from the similar
503 XRD patterns obtained in this study and from other Gulf Coast samples (Perry and Hower,
504 1970, 1972). The diagenetic smectite-to-illite sequences described by the latter authors start
505 from very smectitic material and subsequently evolve to form parageneses having XRD
506 patterns very similar to those of group I samples (fig. 3).
507 *Group I samples: new description of smectite illitization during the first stage.*– From
508 the present interpretation of XRD patterns, the shallow part of the diagenetic smectite-to-illite

509 sequence thus corresponds to the formation of a randomly interstratified I-Exp with prevailing
510 illite layers (W_I > 50%) at the expense of smectite which is present as a pure phase in the
511 shallowest samples. At burial depths lower than 4000 m, the overall smectite-to-illite
512 conversion thus results i) from the dissolution of pure smectite, and ii) from the formation of
513 the randomly interstratified I-Exp with $W_I > W_{Exp}$. The latter process is likely fed by smectite
514 dissolution and favored by K-availability. The overall (I-Exp + smectite) content decreases
515 with increasing burial depth (from ~70% in sample A to ~60% in sample C) possibly because
516 smectite dissolution does not only feed I-Exp formation. Several important conclusions derive
517 from these results.

518 The first stage of smectite illitization is heterogeneous, with the simultaneous progress
519 of smectite dissolution and of I-Exp illitization, in agreement with electron microscopy
520 observation of Gulf Coast shales (Dong and others, 1997; Dong, 2005; Freed and Peacor,
521 1992). As a consequence, pure smectite is present at significant burial depth, indicating a
522 much higher stability than commonly accepted. In the Carter well for example, pure smectite
523 which accounts for most of the clay fraction at 683 m (Berger and others, 1999) persists down
524 to ~4000 m depth where it still represents 2% of the clay fraction (table 5). Although in the
525 investigated samples smectite illitization proceeds simultaneously with partial smectite
526 dissolution, the two reactions do not appear to be systematically linked. For example, Claret
527 and others (2004) presented evidence that I-Exp composition is constant while smectite is
528 steadily dissolving over a narrow depth interval in the Callovo-Oxfordian formation (eastern
529 Paris basin). Similarly, McCarty (2005) and McCarty and others (2008) describe important
530 variations of discrete smectite relative proportion without any compositional evolution of the
531 coexisting I-Exp.

532 The new description also raises the need to reconsider the kinetics of smectite
533 illitization. According to the usual identification criteria (for example Srodon, 1981; Inoue

534 and others, 1989), XRD data obtained from the Carter samples correspond to an I-Exp with ~
535 20% illite layers (R = 0) down to ~2000 m depth (Velde and Vasseur, 1992; Berger and
536 others, 1999). Similarly, shallow samples from Gulf Coast wells are dominated by randomly
537 interstratified I-Exp with ~25% illite layers according to Perry and Hower (sample E-1829 m
538 - 1970, 1972). By contrast, XRD profile modeling shows that I-Exp contains 57% illite layers
539 at similar depth (sample A). Illitization is thus faster than commonly assumed as randomly
540 interstratified I-Exp with $W_I > W_{Exp}$ likely forms under shallow burial conditions consistent
541 with the TEM observations of Freed and Peacor (1992). The formation of a randomly
542 interstratified I-Exp having a given composition thus occurs at much lower temperature than
543 assumed from the commonly accepted model of smectite illitization for similar conditions of
544 burial diagenesis (temperature, pressure, K activity, water-rock ratio, et cetera). The illite
545 content in I-Exp obtained from both approaches may however be partially reconciled by
546 taking into account the contribution of pure smectite. When this contribution is minimum (2%
547 – sample C), similar compositions are determined for I-Exp (~65%I) using either the usual
548 identification criteria (3500-4000 m deep samples in Carter well, fig. 1 – Velde and Vasseur,
549 1992; Berger and others, 1999) or the present modeling approach.
550 In any case, the rate of smectite illitization strongly decreases with increasing burial
551 depth, in contrast with the commonly accepted model (see for example Srodon and Eberl,
552 1984). According to the present data, the illite content in I-Exp increases at a minimum rate of
553 40%I/km from 683 to 2170 m depth. By contrast, from 2170 m to 4000 m the increase of illite
554 content in I-Exp is limited to ~10% (table 4), at a rate of ~5%I/km. In agreement with Berger
555 and others (1999), this rate decrease is likely due to the low amount of available K, in relation
556 with the dissolution of K-feldspars and micas. In the studied samples, the maximum
557 illitization rate coincides with the dissolution of K-feldspars which disappear at ~2000 m in
558 the Carter well (Berger and others, 1999).

559 *Structural evolution of clay minerals during deep burial diagenesis (group II samples).–*
560 The presence of a unique illite-rich ordered ($R \geq 1$) I-Exp is characteristic of deep burial
561 diagenesis in the commonly accepted model for smectite illitization. According to the present
562 modeling results, such a phase is actually present in group II samples coexisting with another
563 illite-containing mixed layer. In addition to illite and Exp layers, the latter structure includes
564 di-trioctahedral chlorite layers, whose formation is consistent with the low K-availability
565 (Whitney and Northrop, 1988) and whose relative proportion increases slightly with
566 increasing burial depth (table 4). Interstratification of the different layer types is almost
567 random in I-Exp-Ch, with only a slight tendency to segregation of Ch layers. By contrast, the
568 slight increase of the illite content in I-Exp is associated with a steady increase of layer
569 ordering. Specifically, the succession of dominant illite layers is favored and the extent of this
570 ordering (quantified by the Reichweit R parameter – Jagodzinski, 1949; Reynolds, 1980)
571 tends to increase beyond the nearest neighbor with increasing burial depth (table 4).
572 *Transition from group I to group II samples: structural evolution of I-Exp from group I*
573 *to group II samples.–* The illite content in I-Exp increases only slightly from sample C to
574 sample D, whereas the layer distribution is dramatically modified between the two samples,
575 interstratification being random in sample C and ordered (R =1 with MPDO) in sample D. In
576 the context of smectite illitization, II pairs should be preserved and solid-state transformation
577 can be hypothesized only if the relative proportion of IExp and ExpI pairs increases at the
578 expense of the sole ExpExp pairs. On the contrary, it is clear from table 6 that ExpExp pairs
579 originally present in sample C are not abundant enough (0.109) to account for the increase of
580 IExp and ExpI pairs from sample C to sample D [$(W_{IExp} + W_{ExpI})_D - (W_{IExp} + W_{ExpI})_C$ =
581 0.158]. The transition from sample C to sample D can thus only result from a dissolution-
582 recrystallization process. Indirect support for the proposed mechanism comes from the
583 extremely low intensity scattered by sample D which required a seven-fold increase of the

584 collection time to obtain a similar signal-to-noise ratio for a given amount of material. The
585 low amplitude of the XRD signal is likely due to the presence of XRD-amorphous material
586 whose presence is expected for a major dissolution-reprecipitation process. Additional
587 indirect support arises from the significant CSDS increase observed for the I-Exp from
588 sample C to sample D (table 5). No K-Ar ages are available for the samples investigated in
589 the present study. However, Aronson and Hower (1976) reported significantly younger ages
590 for deep Gulf Coast samples (typical of group II samples) than for shallower samples (typical
591 of group I samples). The gap between the two groups of samples also supports a major
592 dissolution-recrystallization process leading to the crystallization of an ordered I-Exp at the
593 expense of a randomly interstratified I-Exp of similar composition.
594 *Transition from group I to group II samples: possible solid-state formation of I-Exp-Ch*
595 *at the expense of I-Exp.*– The illite contents in I-Exp from sample C and in I-Exp-Ch from
596 sample D are similar (67 and 70%I, respectively). Their junction probability parameters
597 exhibit also strong similarities, interstratification being random in I-Exp from sample C, and
598 showing only slight tendency to segregation in I-Exp-Ch from sample D (table 4C). In
599 addition, I-Exp from sample C and I-Exp-Ch from sample D have similar CSDSs. It is thus
600 possible to hypothesize a solid-state mechanism, involving Mg polymerization in former Exp
601 interlayers, for the transition between the two mixed layers. In this case, a series of mixed
602 layers with compositions intermediate between those of the two end members can be
603 envisaged. In I-Exp from sample C and in I-Exp-Ch from sample D, Exp layers are randomly
604 distributed within crystallites ($P_{Expi} = W_i$), whereas I and Ch layers are slightly segregated in
605 sample D ($W_I < P_{II}$, and $W_{Ch} < P_{ChCh}$). The degree of segregation of I and Ch layers in I-Exp-
606 Ch from sample D is 0.083 and 0.135, respectively (Eq. 1 – table 4C). To propose
607 compositional and structural parameters for intermediate phases, one may thus hypothesize
608 that the increase of I and Ch contents from sample C to sample D is accompanied by the

609 increase of their tendency to segregation. Probability parameters describing such theoretical
610 intermediate phases (phases I and II) are reported in table 7. In particular, the relative
611 proportions of I and Ch layers in these phases are equal to 68% and 5% (phase I) and 69%
612 and 10% (phase II), respectively, to account for the compositional change from sample C
613 (67%I and 0%Ch) to sample D (70%I and 15%Ch). In addition, the degrees of segregation of
614 I and Ch layers increase steadily from sample C (0.000 and 0.000, random interstratification)
615 to phase I (0.027 and 0.045), to phase II (0.054 and 0.090), and finally to sample D (0.083 and
616 0.135, respectively). Exp layers are randomly distributed in both intermediate phases so that
617 $P_{ExpExp} = W_{Exp}$, $P_{ExpI} = W_I$ and $P_{ExpCh} = W_{Ch}$ as in I-Exp from sample C and in I-Exp-Ch from
618 sample D. Possible mechanisms of the hypothesized solid-state transformation of I-Exp from
619 sample C to I-Exp-Ch from sample D through intermediate I-Exp-Ch phases are detailed in
620 the Appendix.
621
622 CONCLUDINGS REMARKS
623
624 *A General Pattern for Diagenetic Smectite-to-Illite Transition in Shales*
625 The XRD patterns obtained from the Carter well samples are typical for the diagenetic
626 smectite-to-illite transition (fig. 3). The multi-specimen method led however to an unusual
627 description of the data. In particular, an original clay paragenesis is reported and a novel
628 diagenetic evolution of this paragenesis proposed which includes two stages of smectite
629 illitization.
630 In the first stage, the clay paragenesis corresponds to the physical mixture of discrete
631 smectite and of a randomly interstratified I-Exp with a high content of illite layers ($W_I > 50\%$)
632 in addition to illite, kaolinite, chlorite and K-Exp. With increasing burial depth, the relative
633 proportion of I-Exp increases, essentially at the expense of discrete smectite, and its

composition becomes slightly more illitic. Several conclusions in this study contradict the conventional wisdom of smectite-to-illite transition:

- Smectite illitization is a heterogeneous reaction involving the physical mixture of pure smectite and I-Exp.
- Discrete smectite and I-Exp are authigenic.
- The apparent stability of smectite is higher than commonly assumed as this mineral persists down to 4000 m, although its relative abundance decreases with increasing depth.
- Smectite illitization occurs very early and randomly interstratified I-Exp with $W_I > W_{Exp}$ is formed at shallow burial depth, the temperature at which a I-Exp with a given composition is formed being lower than commonly assumed.
- Smectite illitization rate decreases rapidly, most likely as the result of K-feldspar dissolution.

In the second stage of smectite illitization (below 4000 m depth in the present case study), clay paragenesis consists of two illite-containing mixed layers in addition to illite, kaolinite, chlorite and K-Exp. These two illite-containing mixed layers result from two parallel reaction mechanisms affecting the randomly interstratified I-Exp present in the upper part of the series. The first reaction implies the dissolution of the I-Exp and the crystallization of an ordered I-Exp with R = 1 (MPDO) without significant increase of the I layer content (70% versus 67%, tables 4A, 4C), possibly as the result of low K-availability. With increasing depth, ordering increases together with a marginal increase of the I layer content (up to 75% in sample F – table 4C). The second reaction affects the remaining fraction of the randomly interstratified I-Exp and implies the polymerization and growth of trioctahedral brucite-like sheets in Exp interlayers, thus developing di-trioctahedral chlorite layers in the initial I-Exp to form an I-Exp-Ch. A possible layer-by-layer mechanism is supported for this reaction by the random layer distribution in the I-Exp-Ch, similar to that of the initial I-Exp. In this scheme,

659 Mg cations released by the dissolution-recrystallization of I-Exp likely represent the Mg
660 source for the formation of brucite-like sheets.
661
662 **ACKNOWLEDGMENTS**
663
664 The results presented in the present article were collected during a Ph.D. thesis granted
665 by Andra (French National Agency for Nuclear Waste Disposal) to FC. Financial support
666 from Andra (BL and FC), CNRS/PICS709 program (BL, VAD and BAS), and Russian
667 Science Foundation (VAD and BAS) is gratefully acknowledged. Investigated Gulf Coast
668 samples were kindly provided by Bruce Velde (Paris, France). Eric Ferrage and Alain
669 Meunier (Poitiers, France) are thanked for their comments on an early version of the
670 manuscript. Constructive reviews by Neil Tabor, Warren Huff, and Denny Eberl significantly
671 improved the initial version of this manuscript.
672
673 **REFERENCES**
674
675 Altaner, S. P., and Ylagan, R. F., 1997, Comparison of structural models of mixed-layer
676 illite/smectite and reaction mechanisms of smectite illitization: Clays & Clay
677 Minerals, v. 45, p. 517-533.
678 Altaner, S. P., Ylagan, R. F., Savin, S. M., Aronson, J. L., Belkin, H. E., and Pozzuoli, A.,
679 2003, Geothermometry, geochronology, and mass transfer associated with
680 hydrothermal alteration of a rhyolitic hyaloclastite from Ponza Island, Italy:
681 Geochimica Et Cosmochimica Acta, v. 67, p. 275-288.
682 Aplin, A. C., Matenaar, I. F., McCarty, D. K., and van Der Pluijm, B. A., 2006, Influence of
683 mechanical compaction and clay mineral diagenesis on the microfabric and pore-scale

684 properties of deep-water Gulf of Mexico Mudstones.: Clays & Clay Minerals, v. 54, p.
685 500-514.
686 Aronson, J. L., and Hower, J., 1976, The mechanism of burial metamorphism of argillaceous
687 sediments: 2. radiogenic argon evidence: Geological Society of America Bulletin, v.
688 87, p. 738-744.
689 Bauer, A., and Velde, B., 1999, Smectite transformation in high molar KOH solutions: Clay
690 Minerals, v. 34, p. 259-273.
691 Berger, G., Velde, B., and Aigouy, T., 1999, Potassium sources and illitization in Texas Gulf
692 Coast shale diagenesis: Journal of Sedimentary Research, v. 69, p. 151-157.
693 Bethke, C. G., and Altaner, S. P., 1986, Layer-by-layer mechanism of smectite illitization and
694 application to a new rate law: Clays & Clay Minerals, v. 34, p. 136-145.
695 Bethke, C. G., Vergo, N., and Altaner, S. P., 1986, Pathways of smectite illitization: Clays &
696 Clay Minerals, v. 34, p. 125-135.
697 Billault, V., Beaufort, D., Patrier, P., and Petit, S., 2002, Crystal-chemistry of Fe-sudoites
698 from Uranium deposits in the Athabasca basin (Saskatchewan, Canada): Clays & Clay
699 Minerals, v. 50, p. 70-81.
700 Boles, J. R., and Francks, G. S., 1979, Clay diagenesis in Wilcox sandstones of Southwest
701 Texas: Implications of smectite diagenesis on sandstone cementation: Journal of
702 Sedimentary Petrology, v. 49, p. 55-70.
703 Brindley, G. W., Suzuki, T., and Thiry, M., 1983, Interstratified kaolinite/smectites from the
704 Paris Basin; Correlations of layer proportions, chemical compositions and other data:
705 Bulletin de Minéralogie, v. 106, p. 403-410.
706 Burst, J. F., 1957, Postdiagenetic clay mineral environmental relationships in the Gulf Coast
707 Eocene: Clays & Clay Minerals, v. 6, p. 327-341.

-, 1969, Diagenesis of Gulf Coast clayey sediments and its possible relation to petroleum migration: American Association of Petroleum Geologists Bulletin, v. 53, p. 73-93.

Chen, Z. S., Tsou, T. C., Asio, V. B., and Tsai, C. C., 2001, Genesis of inceptisols on a volcanic landscape in Taiwan: Soil Science, v. 166, p. 255-266.

Claret, F., 2001, Caractérisation structurale des transitions minéralogiques dans les formations argileuses : Contrôles et implications géochimiques des processus d'illitisation. Cas particulier d'une perturbation alcaline dans le Callovo-Oxfordien Laboratoire souterrain Meuse-Haute-Marne, Environnemental and Geochimistry Group: Grenoble, France, Université Joseph Fourrier, p. 174.

Claret, F., Sakharov, B. A., Drits, V. A., Velde, B., Meunier, A., Griffault, L., and Lanson, B., 2004, Clay minerals in the Meuse-Haute marne underground laboratory (France): Possible influence of organic matter on clay mineral evolution: Clays and Clay Minerals, v. 52, p. 515-532.

Dong, H., 2005, Interstratified illite-smectite: A review of contributions of TEM data to crystal chemical relations and reaction mechanisms: Clay Science, v. 12, Supp. 1, p. 6-12.

Dong, H., Peacor, D. R., and Freed, R. L., 1997, Phase relations among smectite, R1 illite-smectite, and illite: American Mineralogist, v. 82, p. 379-391.

Douglas, L. A., 1989, Vermiculites, *in* Dixon, J. B., and Weed, S. B., editors, Minerals in Soil Environments: Madison, WI, Soil Science Society of America, p. 635-728.

Drits, V. A., and Sakharov, B. A., 1976, X-Ray structure analysis of mixed-layer minerals: Moscow, Nauka, 256 p.

Drits, V. A., and Tchoubar, C., 1990, X-ray diffraction by disordered lamellar structures: Theory and applications to microdivided silicates and carbons: Berlin, Springer-Verlag, 371 p.

733 Drits, V. A., Varaxina, T. V., Sakharov, B. A., and Plançon, A., 1994, A simple technique for
734 identification of one-dimensional powder X-ray diffraction patterns for mixed-layer
735 illite-smectites and other interstratified minerals: Clays & Clay Minerals, v. 42, p.
736 382-390.
737 Drits, V. A., Lindgreen, H., Sakharov, B. A., and Salyn, A. L., 1997a, Sequence structure
738 transformation of illite-smectite-vermiculite during diagenesis of Upper Jurassic
739 shales, North Sea: Clay Minerals, v. 32, p. 351-371.
740 Drits, V. A., Srodon, J., and Eberl, D. D., 1997b, XRD measurement of mean crystallite
741 tickness of illite and illite/smectite : Reappraisal of the Kubler index and the Scherrer
742 equation: Clays and Clays Minerals, v. 45, p. 461-475.
743 Drits, V. A., Lindgreen, H., Sakharov, B. A., Jakobsen, H. J., Salyn, A. L., and Dainyak, L.
744 G., 2002a, Tobelitization of smectite during oil generation in oil-source shales.
745 Application to North Sea illite-tobelite-smectite-vermiculite: Clays and Clay Minerals,
746 v. 50, p. 82-98.
747 Drits, V. A., Sakharov, B. A., Dainyak, L. G., Salyn, A. L., and Lindgreen, H., 2002b,
748 Structural and chemical heterogeneity of illite-smectites from Upper Jurassic
749 mudstones of East Greenland related to volcanic and weathered parent rocks:
750 American Mineralogist, v. 87, p. 1590-1606.
751 Drits, V. A., Lindgreen, H., Sakharov, B. A., Jakobsen, H. J., and Zviagina, B. B., 2004, The
752 detailed structure and origin of clay minerals at the cretaceous/tertiary boundary,
753 Stevns Klint (Denmark): Clay Minerals, v. 39, p. 367-390.
754 Drits, V. A., Lindgreen, H., Sakharov, B. A., Jakobsen, H. J., Fallick, A. E., Salyn, A. L.,
755 Dainyak, L. G., Zviagina, B. B., and Barfod, D. N., 2007, Formation and
756 transformation of mixed-layer minerals by tertiary intrusives in cretaceous mudstones,
757 West Greenland: Clays and Clay Minerals, v. 55, p. 260-283.

758 Ferrage, E., Lanson, B., Malikova, N., Plancon, A., Sakharov, B. A., and Drits, V. A., 2005a,
759 New insights on the distribution of interlayer water in bi-hydrated smectite from X-ray
760 diffraction profile modeling of 00l reflections: Chemistry of Materials, v. 17, p. 3499-
761 3512.
762 Ferrage, E., Lanson, B., Sakharov, B. A., and Drits, V. A., 2005b, Investigation of smectite
763 hydration properties by modeling experimental X-ray diffraction patterns: Part I.
764 Montmorillonite hydration properties: American Mineralogist, v. 90, p. 1358-1374.
765 Ferrage, E., Lanson, B., Sakharov, B. A., Geoffroy, N., Jacquot, E., and Drits, V. A., 2007,
766 Investigation of dioctahedral smectite hydration properties by modeling of X-ray
767 diffraction profiles: Influence of layer charge and charge location: American
768 Mineralogist, v. 92, p. 1731-1743.
769 Freed, R. L., and Peacor, D. R., 1992, Diagenesis and the formation of authigenic illite-rich
770 I/S crystals in Gulf Coast shales: TEM study of clay separates: Journal of Sedimentary
771 Petrology, v. 62, p. 220-234.
772 Hoffman, J., and Hower, J., 1979, Clay mineral assemblages as low grade metamorphic
773 geothermometers: Application to the thrust faulted disturbed belt of Montana, U.S.A.,
774 *in* Scholle, P. A., and Schluger, R. P., editors, Aspects of Diagenesis: SEPM Special
775 Publication: Tulsa, Oklahoma, p. 55-79.
776 Howard, S. A., and Preston, K. D., 1989, Profile fitting of powder diffraction patterns, *in*
777 Bish, D. L., and Post, J. E., editors, Modern Powder Diffraction: Reviews in
778 Mineralogy: Wahington D.C., Mineralogical Society of America, p. 217-275.
779 Hower, J., Eslinger, E. V., Hower, M. E., and Perry, E. A., 1976, Mechanism of burial
780 metamorphism of argillaceous sediments: 1. Mineralogical and chemical evidence:
781 Geological Society of America Bulletin, v. 87, p. 725-737.

782 Huang, W. L., 1993, The formation of illitic clays from kaolinite in KOH solution from
783 225°C to 350°C: Clays & Clay Minerals, v. 41, p. 645-654.
784 Inoue, A., and Utada, M., 1983, Further investigations of a conversion series of dioctahedral
785 mica/smectites in the Shinzan hydrothermal alteration area, northeast Japan: Clays &
786 Clay Minerals, v. 31, p. 401-412.
787 Inoue, A., Minato, H., and Utada, M., 1978, Mineralogical properties and occurrence of
788 illite/montmorillonite mixed layer minerals formed from Miocene volcanic glass in
789 Waga-Omono district: Clay Science, v. 5, p. 123-136.
790 Inoue, A., Velde, B., Meunier, A., and Touchard, G., 1988, Mechanism of illite formation
791 during smectite-to-illite conversion in a hydrothermal system: American Mineralogist,
792 v. 73, p. 1325-1334.
793 Inoue, A., Bouchet, A., Velde, B., and Meunier, A., 1989, Convenient technique for
794 estimating smectite layer percentage in randomly interstratified illite/smectite
795 minerals: Clays & Clay Minerals, v. 37, p. 227-234.
796 Inoue, A., Watanabe, T., Kohyama, N., and Brusewitz, A. M., 1990, Characterization of
797 illitization of smectite in bentonite beds at Kinnekulle, Sweden: Clays & Clay
798 Minerals, v. 38, p. 241-249.
799 Inoue, A., Lanson, B., Marques Fernandes, M., Sakharov, B. A., Murakami, T., Meunier, A.,
800 and Beaufort, D., 2005, Illite-smectite mixed-layer minerals in the hydrothermal
801 alteration of volcanic rocks: I. One-dimensional XRD structure analysis and
802 characterization of component layers: Clays and Clay Minerals, v. 53, p. 423-439.
803 Jagodzinski, H., 1949, Eindimensionale Fehlordnung in Kristallen und ihr Einfluss auf die
804 Röntgeninterferenzen: I. Berechnung des Fehlordnungsgrades aus der
805 Röntgenintensitaten: Acta Crystallographica, v. 2, p. 201-207.

806 Jennings, S., and Thompson, G. R., 1986, Diagenesis of Plio-Pleistocene sediments of the
807 Colorado river delta, southern California: Journal of Sedimentary Petrology, v. 56, p.
808 89-98.
809 Kameda, J., Miyawaki, R., Kitagawa, R., and Kogure, T., 2007, XRD and HRTEM analyses
810 of stacking structures in sudoite, di-trioctahedral chlorite: American Mineralogist, v.
811 92, p. 1586-1592.
812 Lanson, B., 2005, Crystal structure of mixed-layer minerals and their X-ray identification:
813 New insights from X-ray diffraction profile modeling: Clay Science, v. 12, Supp. 1, p.
814 1-5.
815 Lanson, B., Sakharov, B. A., Claret, F., and Drits, V. A., 2005, Diagenetic evolution of clay
816 minerals in Gulf Coast shales: New insights from X-ray diffraction profile modeling,
817 42nd Annual Meeting, Clay Minerals Society: Burlington, VT, p. 69.
818 Li, G., Peacor, D. R., and Coombs, D. S., 1997, Transformation of smectite to illite in
819 bentonite and associated sediments from Kaka point, New Zealand: Contrast in rate
820 and mechanism: Clays & Clay Minerals, v. 45, p. 54-67.
821 Lin, C. Y., and Bailey, S. W., 1985, Structural data for sudoite: Clays & Clay Minerals, v. 33,
822 p. 410-414.
823 Lindgreen, H., Drits, V. A., Sakharov, B. A., Salyn, A. L., Wrang, P., and Dainyak, L. G.,
824 2000, Illite-smectite structural changes during metamorphism in black Cambrian
825 Alum shales from the Baltic area: American Mineralogist, v. 85, p. 1223-1238.
826 Lindgreen, H., Drits, V. A., Sakharov, B. A., Jakobsen, H. J., Salyn, A. L., Dainyak, L. G.,
827 and Kroyer, H., 2002, The structure and diagenetic transformation of illite-smectite
828 and chlorite-smectite from North Sea Cretaceous-Tertiary chalk: Clay Minerals, v. 37,
829 p. 429-450.

Marques, J. J., Teixeira, W. G., Schulze, D. G., and Curi, N., 2002, Mineralogy of soils with unusually high exchangeable Al from the western Amazon Region: Clay Minerals, v. 37, p. 651-661.

McCarty, D. K., 2005, XRD pattern simulation of clays and geological interpretation, 42nd Annual Meeting, Clay Minerals Society: Burlington, VT, p. 78.

McCarty, D. K., Drits, V. A., Sakharov, B., Zviagina, B. B., Ruffell, A., and Wach, G., 2004, Heterogeneous mixed-layer clays from the Cretaceous greensand, Isle of Wight, southern England: Clays and Clay Minerals, v. 52, p. 552-575.

McCarty, D. K., Drits, V. A., and Sakharov, B. A., 2005, Advantages and limitations of simulation of XRD patterns of clays: Mod-1 to present, 42nd Annual Meeting, Clay Minerals Society: Burlington, VT, p. 76.

McCarty, D. K., Sakharov, B. A., and Drits, V. A., 2008, Early clay diagenesis in Gulf Coast sediments: New insights from XRD profile modeling: Clays & Clay Minerals, p. in press.

Méring, J., 1949, L'interférence des rayons-X dans les systèmes à stratification désordonnée: Acta Crystallographica, v. 2, p. 371-377.

Moore, D. M., and Reynolds, R. C., Jr, 1997, X-ray Diffraction and the Identification and Analysis of Clay Minerals, Oxford University Press, 378 p.

Nadeau, P. H., and Reynolds, R. C., Jr, 1981, Burial and contact metamorphism in the Mancos Shale: Clays & Clay Minerals, v. 29, p. 249-259.

Perry, E. A., Jr, and Hower, J., 1970, Burial diagenesis in Gulf Coast pelitic sediments: Clays & Clay Minerals, v. 18, p. 165-177.

-, 1972, Late-stage dehydration in deeply buried pelitic sediments: American Association of Petroleum Geologists Bulletin, v. 56, p. 2013-2021.

Pytte, A. M., and Reynolds, R. C., 1989, The thermal transformation f smectite to illite, *in* Naeser, N. D., and McCulloh, T. H., editors, Thermal history of sedimentary basins: New York, Springer, p. 133-140.

Reynolds, R. C., Jr, 1967, Interstratified clay systems: Calculation of the total one-dimensional diffraction function: American Mineralogist, v. 52, p. 661-672.

-, 1980, Interstratified clay minerals, *in* Brindley, G. W., and Brown, G., editors, Crystal structures of clay minerals and their X-ray identification: London, The Mineralogical Society, p. 249-359.

-, 1986, The Lorentz-polarization factor and preferred orientation in oriented clay aggregates: Clays & Clay Minerals, v. 34, p. 359-367.

Reynolds, R. C., Jr, and Hower, J., 1970, The nature of interlayering in mixed-layer illite-montmorillonites: Clays & Clay Minerals, v. 18, p. 25-36.

Sakharov, B. A., and Drits, V. A., 1973, Mixed-layer kaolinite-montmorillonite: A comparison of observed and calculated diffraction patterns: Clays & Clay Minerals, v. 21, p. 15-17.

Sakharov, B. A., Lindgreen, H., and Drits, V. A., 1999a, Mixed-layer kaolinite-illite-vermiculite in North Sea shales: Clay Minerals, v. 34, p. 333-344.

Sakharov, B. A., Lindgreen, H., Salyn, A., and Drits, V., 1999b, Determination of illite-smectite structures using multispecimen XRD profile fitting.: Clays and Clays Minerals, v. 47, p. 555-566.

Sakharov, B. A., Dubinska, E., Bylina, P., Kozubowski, J. A., Kapron, G., and Frontczak Baniewicz, M., 2004, Serpentine-smectite interstratified minerals from Lower Silesia (SW Poland): Clays and Clay Minerals, v. 52, p. 55-65.

Shutov, V. D., Drits, V. A., and Sakharov, B. A., 1969, On the mechanism of a postsedimentary transformation of montmorillonite into hydromica, *in* Heller, L.,

879 editor, International Clay Conference: Tokyo, Japan, Israel University Press,
880 Jerusalem, p. 523-531.
881 Srodon, J., 1978, Correlation between coal and clay diagenesis in the Carboniferous of the
882 upper Silesian coal basin, *in* Mortland, M. M., and Farmer, V. C., editors,
883 International Clay Conference: Oxford, Elsevier, p. 251-260.
884 -, 1980, Precise identification of illite/smectite interstratifications by X-ray powder
885 diffraction: Clays & Clay Minerals, v. 28, p. 401-411.
886 -, 1981, X-Ray identification of randomly interstratified illite-smectite in mixtures with
887 discrete illite: Clay Minerals, v. 16, p. 297-304.
888 -, 1984a, Mixed-layer illite-smectite in low-temperature diagenesis: Data from the Miocene of
889 the Carpathian foredeep: Clay Minerals, v. 19, p. 205-215.
890 -, 1984b, X-ray powder diffraction of illitic materials: Clays & Clay Minerals, v. 32, p. 337-
891 349.
892 -, 1999, Nature of mixed-layer clays and mechanisms of their formation and alteration:
893 Annual Review of Earth and Planetary Sciences, v. 27, p. 19-53.
894 Srodon, J., and Eberl, D. D., 1984, Illite, *in* Bailey, S. W., editor, Micas: Reviews in
895 Mineralogy: Washington DC, Mineralogical Society of America, p. 495-544.
896 Srodon, J., Eberl, D. D., and Drits, V. A., 2000, Evolution of fundamental-particle size during
897 illitization of smectite and implications for reaction mechanism: Clays and Clay
898 Minerals, v. 48, p. 446-458.
899 Sucha, V., Kraus, I., Gerthofferova, H., Petes, J., and Serekova, M., 1993, Smectite to illite
900 conversion in bentonites and shales of the East Slovak basin: Clay Minerals, v. 28, p.
901 243-253.
902 Sudo, T., and Shimoda, S., 1977, Interstratified clay minerals - Mode of occurrence and
903 origin: Minerals Sci. Engng., v. 9, p. 3-24.

Velde, B., and Brusewitz, A. M., 1982, Metasomatic and non-metasomatic low grade metamorphism of Ordovician meta-bentonites in Sweden: Geochimica & Cosmochimica Acta, v. 46, p. 447-452.

-, 1986, Compositional variation in component layers in natural illite/smectite: Clays & Clay Minerals, v. 34, p. 651-657.

Velde, B., and Iijima, A., 1988, Comparison of clay and zeolite mineral occurrences in Neogene age sediments from several deep wells: Clays & Clay Minerals, v. 36, p. 337-342.

Velde, B., and Espitalié, J., 1989, Comparison of kerogen maturation and illite/smectite composition in diagenesis: Journal of Petroleum Geology, v. 12, p. 103-110.

Velde, B., and Vasseur, G., 1992, Estimation of the diagenetic smectite to illite transformation in time-temperature space: American Mineralogist, v. 77, p. 967-976.

Velde, B., Suzuki, T., and Nicot, E., 1986, Pressure-Temperature-Composition of illite/smectite mixed-layer minerals: Niger delta mudstones and other examples: Clays & Clay Minerals, v. 34, p. 435-441.

Watanabe, T., 1981, Identification of illite/montmorillonite interstratification by X-ray powder diffraction: Journal of the Mineralogical Society of Japan, v. Spec. Issue 15, p. 32-41.

-, 1988, The structural model of illite/smectite interstratified mineral and the diagram for their identification: Clay Science, v. 7, p. 97-114.

Weaver, C. E., 1957, The clay petrology of sediments: Clays and Clay Minerals, v. 6, p. 154-187.

-, 1959, Possible uses of clay minerals in search for oil: Clays and Clay Minerals, v. 8, p. 214-227.

928 Whitney, G., 1990, Role of water in the smectite-to-illite reaction: Clays & Clay Minerals, v.
929 38, p. 343-350.
930 Whitney, G., and Northrop, H. R., 1988, Experimental investigation of the smectite to illite
931 reaction: Dual reaction mechanisms and oxygen-isotope systematics: American
932 Mineralogist, v. 73, p. 77-90.

933 **FIGURE CAPTIONS**

934

935 Fig. 1. Age of the sediments as a function of depth in Carter and Mustang Island wells
936 (top – Velde and Vasseur, 1992). Smectite content in I-Exp as determined by Velde and
937 Vasseur (1992) as a function of depth in these two wells.

938 Fig. 2. Experimental XRD patterns obtained from Carter well samples selected as being
939 representative of the complete smectite-to-illite diagenetic transition. Sampling depths are
940 2170 (A), 3660 (B), 4000 (C), 4640 (D), 5010 (E), and 5180 m (F). XRD patterns obtained on
941 EG solvated samples. Dashed and dot-dashed lines indicate the positions of illite and smectite
942 reflections. Solid and dot-dot-dashed lines indicate positions of some kaolinite and chlorite
943 reflections. For all samples, the gray bar indicates a modified scale factor for the high-angle
944 region.

945 Fig. 3. Comparison between experimental XRD patterns obtained from Carter well
946 samples investigated in the present study and those obtained by Perry and Hower (1970) on
947 selected samples from well E (Galveston county). The latter samples were used to establish
948 the smectite-to-illite diagenetic transition in Gulf Coast clay-rich sediments. XRD patterns
949 obtained on EG solvated samples.

950 Fig. 4. Comparison between experimental and calculated XRD patterns as a function of
951 depth for group I samples (single-phase segregated I-Exp model). Experimental and
952 calculated optimal XRD patterns are shown as crosses and as solid lines, respectively.
953 Optimal structure models are described in tables 1 and 2. For all samples, the gray bar
954 indicates a modified scale factor for the high-angle region. **A**. XRD patterns obtained on EG
955 solvated samples. **B**. XRD patterns obtained on air-dried samples at 40% relative humidity.

956 Fig. 5. Comparison between experimental and calculated XRD patterns as a function of
957 depth for all Carter well samples (mixture model). Experimental and calculated optimal XRD

patterns are shown as crosses and as solid lines, respectively. Optimal structure models are described in tables 4 and 5. For all samples, the gray bar indicates a modified scale factor for the high-angle region. **A**. XRD patterns obtained on EG solvated samples. **B**. XRD patterns obtained on air-dried samples at 40% relative humidity.

Fig. 6. Sensitivity of calculated XRD patterns to the mineralogical composition. Patterns as for figure 5. Arrows indicate significant misfit as compared to the optimum fits shown in figure 5. The optimum mineralogical composition is given in table 5. **A**. Sample B – 3660 m Ca-saturated after EG solvation without the contribution of discrete smectite. **B**. Sample B – 3660 m Ca-saturated after EG solvation without the contribution of K-Exp.

Fig. 7. Sensitivity of calculated XRD patterns to the mineralogical composition. Patterns as for figure 5. Arrows indicate significant misfit as compared to the optimum fits shown in figure 5. The optimum mineralogical composition is given in table 5. **A**. Sample E – 5010 m Ca-saturated after EG solvation without the contribution of I-Exp. **B**. Sample E – 5010 m Ca-saturated air-dried without the contribution of I-Exp. **C**. Sample E – 5010 m Ca-saturated air-dried without the contribution of I-Exp-Ch.

Fig. 8. Sensitivity of calculated XRD patterns to structural parameters. Patterns as for figure 5. Arrows indicate significant misfit as compared to the optimum fits shown in figure 5. The structural parameters for the optimal models are given in table 4. **A**. Sample E – 5010 m Ca-saturated air-dried. In I-Exp-Ch, Ch layers (with 3.0 Mg and 6.0 OH per half unit-cell in their interlayers) are replaced by Exp layers (with 0.25 Mg and 2.0 OH per half unit-cell in their interlayers). **B**. Sample B – 3660 m Ca-saturated air-dried. In I-Exp, 14.0 Å Exp layers (8% of the layers) are replaced by 15.0 Å Exp layers. **C**. Sample B – 3660 m Ca-saturated air-dried. In I-Exp, 14.0 Å Exp layers (8% of the layers) are replaced by 12.5 Å Exp layers.

Table 1A. Single-phase segregated I-Exp model. Composition and structural parameters of the segregated I-Exp in group I samples.

Sample	W_I	W_{Exp1}	W_{Exp2}	W_{Exp3}	h_{Exp1}	h_{Exp2}	h_{Exp3}	R	N_{av}	N_{max}	S_q
A – EG	0.45	0.55	-	-	16.76	-	-	1	7	50	0.27
A – AD	0.45	0.30	0.15	0.10	15.00	12.50	14.00	1	7	50	
B – EG	0.65	0.27	0.08	-	16.76	14.00	-	1	15	50	0.19
B – AD	0.65	0.21	0.14	-	15.00	12.50	-	1	15	50	
C – EG	0.65	0.27	0.08	-	16.76	14.00	-	1	15	50	0.10
C – AD	0.65	0.15	0.20	-	14.90	12.50	-	1	15	50	

Note: The basal d_{001} distances of the different layer types (h_i) are given in Å. R is the Reichweit parameter (Jagodzinski, 1949) which characterizes the extent of ordering as the number of adjacent layers influencing the nature of a given layer. N_{av} and N_{max} are the average and maximum numbers of layers in coherent scattering domains (lognormal size distribution). S_q parameter is an estimator of the degree of segregation in I-Exp (eq 1).

Table 1B. Single-phase segregated I-Exp model. Junction probabilities of the segregated I-Exp in samples A, B, and C.

A-AD	I 9.98 Å	Exp1 15.00 Å	Exp2 12.50 Å	Exp3 14.00 Å
I (9.98 Å) 0.45	0.600	0.133	0.133	0.133
Exp1 (15.00 Å) 0.30	0.200	0.500	0.167	0.133
Exp2 (12.50 Å) 0.15	0.400	0.333	0.267	0.000
Exp3 (14.00 Å) 0.10	0.600	0.400	0.000	0.000

A-EG	I 9.98 Å	Exp 16.76 Å
I (9.98 Å) 0.45	0.600	0.400
Exp (16.76 Å) 0.55	0.327	0.673

B-AD	I 9.98 Å	Exp1 15.00 Å	Exp2 12.50 Å
I (9.98 Å) 0.65	0.716	0.178	0.106
Exp1 (15.00 Å) 0.21	0.520	0.350	0.130
Exp2 (12.50 Å) 0.14	0.537	0.150	0.313

B-EG	I 9.98 Å	Exp1 16.76 Å	Exp2 14.00 Å
I (9.98 Å) 0.65	0.716	0.216	0.068
Exp1 (16.76 Å) 0.27	0.520	0.480	0
Exp2 (14.00 Å) 0.08	0.550	0	0.450

C-AD	I 9.98 Å	Exp1 15.00 Å	Exp2 12.50 Å
I (9.98 Å) 0.65	0.684	0.138	0.178
Exp1 (14.90 Å) 0.15	0.600	0.150	0.250
Exp2 (12.50 Å) 0.20	0.580	0.240	0.180

C-EG	I 9.98 Å	Exp1 16.76 Å	Exp2 14.00 Å
I (9.98 Å) 0.65	0.683	0.249	0.068
Exp1 (16.76 Å) 0.27	0.600	0.400	0
Exp2 (14.00 Å) 0.08	0.550	0	0.450

Table 2. Single-phase segregated I-Exp model. Relative proportions (in wt%) of the different contributions to the diffracted intensity.

Sample	I-Exp	Ill	Kaol	Ch	K-Exp[a]	R_{wp}[b]	R_{exp}[b]
A – EG	79	5	11	-	5	11.42%	1.73%
A – AD	79	5	11	-	5	11.00%	1.64%
B – EG	64	10	9	1	16	11.60%	2.36%
B – AD	57	13	9	2	19	10.80%	2.05%
C – EG	55	18	8	1	18	11.31%	1.94%
C – AD	52	25	8	2	13	9.85%	1.85%

[a] The composition of K-Exp is constant (75:25 K:Exp ratio).
[b] Estimators of the fit quality (R_{wp}) and of the statistical error associated with measured intensities (R_{exp} – Howard and Preston, 1989)).

Table 3. Single-phase segregated I-Exp model. Relative abundance of the different layers and layer pairs (W_i and W_{ij} parameters) for the segregated I-Exp in group I samples.

Layer sequence	A sample	B sample	C sample
I	0.45	0.65	0.65
Exp	0.55	0.35	0.35
II	0.270	0.465	0.444
IExp	0.180	0.184	0.206
ExpI	0.180	0.184	0.206
ExpExp	0.370	0.166	0.144

Table 4A. Mixture model. Composition and structural parameters of I-Exp in group I samples.

Sample	Phase	W_I	W_{Exp1}	W_{Exp2}	W_{Exp3}	h_{Exp1}	h_{Exp2}	h_{Exp3}	N_{av}	N_{max}	R	Junction probability parameters
A – EG	I-Exp	0.57	0.35	0.08	-	16.70	14.00	-	12	50	0	R = 0 ($P_{ij} = W_j$)
A – AD	I-Exp	0.57	0.20	0.08	0.15	15.00	14.00	12.50	12	50	0	-
B – EG	I-Exp	0.62	0.30	0.08	-	16.72	14.00	-	12	50	0	-
B – AD	I-Exp	0.62	0.15	0.08	0.15	15.00	14.00	12.50	12	50	0	-
C – EG	I-Exp	0.67	0.30	0.03	-	16.85	14.00	-	12	50	0	-
C – AD	I-Exp	0.67	0.17	0.03	0.13	15.00	14.00	12.50	12	50	0	-

The basal d_{001} distances of the different layer types (h_i) are given in Å. R is the Reichweit parameter (Jagodzinski, 1949) which characterizes the extent of ordering as the number of adjacent layers influencing the nature of a given layer. N_{av} and N_{max} are the average and maximum numbers of layers in coherent scattering domains (lognormal size distribution).

Table 4B. Mixture model. Composition and structural parameters of K-Exp.

Sample	Phase	W_I	W_{Exp1}	W_{Exp2}	H_K	h_{Exp1}	h_{Exp2}	N_{av}	N_{max}	R	Junction probability parameters
A – EG	K-Exp	0.75	0.10	0.15	7.156	16.90	12.90	12	50	0	R = 0 ($P_{ij} = W_j$)
A – AD	K-Exp	0.75	0.05	0.20	7.156	15.00	12.50	12	50	0	-
B – EG	K-Exp	0.75	0.00	0.25	7.156	16.90	12.90	12	50	0	-
B – AD	K-Exp	0.75	0.00	0.25	7.156	15.00	12.50	12	50	0	-
C – EG	K-Exp	0.75	0.10	0.15	7.156	16.90	12.90	12	50	0	-
C – AD	K-Exp	0.75	0.00	0.25	7.156	15.00	12.50	12	50	0	-
D – EG	K-Exp	0.75	0.15	0.10	7.156	16.90	12.90	12	50	0	-
D – AD	K-Exp	0.75	0.05	0.20	7.156	15.00	12.50	12	50	0	-
E – EG	K-Exp	0.75	0.15	0.10	7.156	16.90	12.90	12	50	0	-
E – AD	K-Exp	0.75	0.00	0.25	7.156	15.00	12.50	12	50	0	-
F – EG	K-Exp	0.75	0.10	0.15	7.156	16.90	12.90	12	50	0	-

The basal d_{001} distances of the different layer types (h_i) are given in Å. R is the Reichweit parameter (Jagodzinski, 1949) which characterizes the extent of ordering as the number of adjacent layers influencing the nature of a given layer. N_{av} and N_{max} are the average and maximum numbers of layers in coherent scattering domains (lognormal size distribution).

Table 4C. Mixture model. Composition and structural parameters of the mixed layers in group II samples.

Sample	Phase	W_I	W_{Exp1}	W_{Exp2}	W_{Ch}	h_{Exp1}	h_{Exp2}	h_{Ch}	N_{av}	N_{max}	R	Junction probability parameters
D – EG	I-Exp	0.70	0.25	0.05		16.86	12.90		15	100	1	R = 1 with MPDO[a] $P_{Exp1Exp1} = P_{Exp1Exp2} = 0$ $P_{Exp2Exp1} = P_{Exp2Exp2} = 0$
	I-Exp-Ch	0.70	0.15	-	0.15	16.86		14.00[b]	12	50	1	$P_{Exp1Exp1} = P_{Exp1Ch} = P_{ChExp1} = 0.150$ $P_{ChCh} = 0.265$
D – AD	I-Exp	0.70	0.30			15.00			15	100	1	R = 1 with MPDO[a] $P_{Exp1Exp1} = 0$
	I-Exp-Ch	0.70	0.05	0.10	0.15	15.00	12.50	14.00[b]	12	50	1	$P_{Exp1Exp1} = P_{Exp2Exp1} = P_{ChExp1} = 0.050$ $P_{Exp1Exp2} = P_{Exp2Exp2} = P_{ChExp2} = 0.100$ $P_{Exp1Ch} = P_{Exp2Ch} = 0.150$ $P_{ChCh} = 0.265$
E – EG	I-Exp	0.75	0.21	0.04		16.92	12.90		15	100	2	$P_{Exp1Exp1} = P_{Exp1Exp2} = P_{Exp2Exp1} = P_{Exp2Exp2} = 0$ $P_{Exp1IExp1} = 0.350$[b]
	I-Exp-Ch	0.70	0.15		0.15	16.86		14.00[b]	12	50	1	$P_{Exp1Exp1} = P_{Exp1Ch} = P_{ChExp1} = 0.150$ $P_{ChCh} = 0.265$
E – AD	I-Exp	0.75	0.21	0.04		15.00	12.50		15	100	2	$P_{Exp1Exp1} = P_{Exp1Exp2} = P_{Exp2Exp1} = P_{Exp2Exp2} = 0$ $P_{Exp1IExp1} = 0.350$[b]
	I-Exp-Ch	0.70		0.15	0.15		12.50	14.00[b]	12	50	1	$P_{Exp1Exp1} = P_{Exp1Ch} = P_{ChExp1} = 0.150$ $P_{ChCh} = 0.265$
F – EG	I-Exp	0.75	0.20	0.05		16.86	12.90		15	100	2	$P_{Exp1Exp1} = P_{Exp1Exp2} = P_{Exp2Exp1} = P_{Exp2Exp2} = 0$

I-Exp-Ch	0.70	0.10		0.20	16.86		14.00[b]	12	50	1	$P_{Exp1IExp1}$ = 0.300, $P_{Exp1IExp2}$ = 0.050[c] $P_{Exp1Exp1}$ = P_{Exp1Ch} = P_{ChExp1} = 0.150 P_{ChCh} = 0.265

[a] Maximum possible degree of ordering which prohibits pairs of the minor layers: P_{jj} = 0 if W_j <0.5. Refer to Reynolds (1980), Drits and Tchoubar (1990), and Moore and Reynolds (1997) for additional details.

[b] Other junction probability parameters needed to describe layer stacking are $P_{Exp1IExp2}$ = $P_{Exp2IExp1}$ = $P_{Exp2IExp2}$ = 0

[c] Other junction probability parameters needed to describe layer stacking are $P_{Exp2IExp1}$ = $P_{Exp2IExp2}$ = 0

Table 5. Mixture model. Relative proportions (in wt%) of the different contributions to the diffracted intensity.

Sample	I-Exp	I-Exp-Ch	Sm	Ill	Kaol	Ch	K-Exp	R_{wp}[a]	R_{exp}[a]
A – EG	45	-	27	4	9	-	15	9.14%	1.73%
A – AD	43	-	26	6	11	-	14	8.06%	1.64%
B – EG	51	-	5	15	14	2	13	14.16%	2.36%
B – AD	50	-	5	19	12	2	12	9.30%	2.05%
C – EG	57	-	2	21	6	2	12	11.12%	1.94%
C – AD	58	-	3	22	7	2	8	9.72%	1.85%
D – EG	42	26	-	10	6	4	12	8.23%	2.28%
D – AD	39	28	-	9	5	4	15	8.99%	1.15%
E – EG	34	30	-	9	11	4	12	10.23%	2.11%
E – AD	31	32	-	6	12	5	14	11.94%	2.00%
F – EG	34	42	-	5	7	5	7	13.38%	3.07%

[a] Estimators of the fit quality (R_{wp}) and of the statistical error associated with measured intensities (R_{exp} – Howard and Preston, 1989).

Table 6. Mixture model. Relative abundance of the different layers and layer pairs (W_i and W_{ij} parameters) in the I-Exp of samples C and D.

Layer sequence	C sample	D sample
I	0.670	0.700
Exp1	0.300	0.250
Exp2	0.030	0.050
II	0.449	0.400
IExp1	0.201	0.250
IExp2	0.020	0.050
Exp1I	0.201	0.250
Exp1Exp1	0.090	0.000
Exp1Exp2	0.009	0.000
Exp2I	0.020	0.050
Exp2Exp1	0.009	0.000
Exp2Exp2	0.001	0.000

Table 7. Mixture model. Junction probabilities of mixed layers occurring during the hypothesized solid-state transformation of I-Exp from sample C to I-Exp-Ch from sample D. The composition and structural parameters (segregation of I and Exp layers) of these mixed layers are thus theoretically intermediate between those of the two end members.

Layer sequence	Sample C	Inter. Phase I	Inter. phase II	Sample D
W_I	0.670	0.680	0.690	0.700
W_{Exp}	0.330	0.270	0.210	0.150
W_{Ch}	0.000	0.050	0.100	0.150
S_q - I	0.000	0.027	0.054	0.083
S_q - Ch	0.000	0.045	0.090	0.135
P_{II}	0.670	0.689	0.707	0.725
P_{IExp}	0.330	0.264	0.205	0.150
P_{ICh}	0.000	0.047	0.088	0.125
P_{ExpI}	0.670	0.680	0.690	0.700
P_{ExpExp}	0.330	0.270	0.210	0.150
P_{ExpCh}	0.000	0.050	0.100	0.150
P_{ChI}	-	0.561	0.573	0.585
P_{ChExp}	-	0.346	0.246	0.150
P_{ChCh}	-	0.093	0.181	0.265

Note: S_q is an estimator of the degree of segregation of I and Ch layers in I-Exp-Ch (eq 1).

APPENDIX

Single-phase segregated I-Exp model: Self-consistency of the model.

For a given sample, junction probability parameters, P_{ij}, refined for the I-Exp contribution are different for AD and EG states (table 1B). This apparent inconsistency arises from the contrasting expansion behavior of Exp layers in AD and EG states. For example, the hydration behavior of Exp layers is highly heterogeneous in sample A with three types of Exp layers, whereas EG solvation results in the homogeneous swelling of all Exp layers to 16.76 Å (2EG). However, the distribution of illite and expandable layers in I-Exp should be identical in both states. Therefore, the four-component I-Exp in sample A (AD state) must be reduced to a two-component system following EG solvation if the 15.0, 14.0 and 12.5 Å layers become 2EG layers. To ensure the consistency of the structure model for sample A the sums ($W_{Exp1I} + W_{Exp2I} + W_{Exp3I}$), ($W_{IExp1} + W_{IExp2} + W_{IExp3}$), and ($W_{Exp1Exp1} + W_{Exp1Exp2} + W_{Exp1Exp3} + W_{Exp2Exp1} + W_{Exp2Exp2} + W_{Exp2Exp3} + W_{Exp3Exp1} + W_{Exp3Exp2} + W_{Exp3Exp3}$) obtained for the four-component I-Exp (AD state) must be equal to the parameters W_{ExpI}, W_{IExp} and W_{ExpExp}, respectively, determined for the two-component I-Exp following EG solvation (table 1B). Here, $W_{ij} = W_i P_{ij}$ is the occurrence probability for an ij layer pair (i, j = I, Exp, Exp_1, Exp_2 and Exp_3 – Exp, Exp_1, Exp_2 and Exp_3 denote 16.76, 15.0, 12.5 and 14.0 Å layers). W_{ij} parameters are reported in table A-1 for I-Exp in group I samples. For sample A, $W_{II} = 0.270$ in both AD and EG states and the above relationships are valid. In samples B and C, two types of expandable layers coexist in both AD and EG states. However, the relative amounts of the two types differ in AD and EG states, thus leading to contrasting values of P_{ij} parameters for the corresponding models (table 1B). To ensure the consistency of the proposed models these parameters can be reconciled by considering that some of the

905 expandable layers (noted as Exp' layers in tables A-1B, C) behave as Exp2 layers in the AD
906 state and as Exp1 layers when EG solvated (tables A-1B, C).
907
908 *Possible solid-state formation of I-Exp-Ch (sample D) at the expense of I-Exp (sample C)*
909 As described in the main text, the contents of illite layers in I-Exp from sample C and in
910 I-Exp-Ch from sample D are similar (67 and 70%I, respectively). Junction probability
911 parameters exhibit also strong similarities, interstratification being random in I-Exp from
912 sample C, and showing only slight tendency to segregation in I-Exp-Ch from sample D (table
913 4). In addition, I-Exp from sample C and I-Exp-Ch from sample D have similar CSD sizes.
914 As a consequence, a solid-state mechanism can be hypothesized for the transition between the
915 two mixed layers, and a series of mixed layers with compositions and structural features (for
916 example the segregation degree of I and Ch Layers, and the random interstratification of Exp
917 layers) intermediate between those of the two end members can be envisaged (table 7). The
918 scope of this section is to describe in detail this hypothesized solid-state transformation and to
919 assess its robustness from the analysis of the relative abundance of layer pairs and triplets
920 (W_{ij}, and W_{ijk}, respectively – i, j, k = I, Exp, Ch) and of their evolution during the
921 transformation. This evolution should follow logically from that of the relative proportion of
922 the different layer types and of their layer stacking.
923 For this purpose, relative abundances of layer pairs and triplets deduced from structure
924 models (W_{XRD} in table A-2) serve as the basis for this analysis. The first step is thus to
925 calculate the occurrence probabilities for layer pairs and triplets in I-Exp from sample C, in I-
926 Exp-Ch from sample D, and in the two intermediate phases. These occurrence probabilities
927 can be calculated from the junction probabilities listed in table 7 ($W_{ij} = W_i P_{ij}$, and $W_{ijk} =$
928 $W_{ij} P_{jk}$) and are reported in table A-2 (columns W_{XRD}). The second step is to identify layer
929 pairs whose occurrence probability deduced from structure models (columns W_{XRD}) is

930 decreasing along the reaction pathway (from I-Exp in sample C to phase I to phase II and
931 finally to I-Exp-Ch in sample D). For example, from I-Exp in sample C to phase I, the
932 occurrence probabilities of IExp, ExpI and ExpExp pairs (W_{IExp}, W_{ExpI}, W_{ExpExp}) are
933 decreasing. In table A-2 such pairs are identified with an arrow following their occurrence
934 probability. The third step is to distribute these layer pairs so as to match the occurrence
935 probabilities of layer pairs in the next phase (phase I in our example) as shown in table A-3A.
936 In our example, 0.1798 out of the initial 0.2211 IExp pairs are preserved whereas 0.0319 pairs
937 are transformed to ICh pair, as required for intermediate phase I, the remaining 0.0094 pairs
938 being transformed to II pairs. The same procedure can be applied to ExpI and ExpExp pairs.
939 As a result, theoretical occurrence probabilities can be calculated for all layer pairs in phase I,
940 phase II, and in the I-Exp-Ch from sample D. These values are reported in the W_{Cal} columns
941 of table A-2, and they systematically coincide with W_{XRD} values. The fourth step is to
942 calculate occurrence probabilities for all layer triplets. Again, this starts with the identification
943 of the layer triplets whose occurrence probability deduced from structure models (columns
944 W_{XRD}) is decreasing along the reaction pathway (from I-Exp in sample C to phase I to phase
945 II and finally to I-Exp-Ch in sample D). For example, from I-Exp in sample C to phase I, the
946 occurrence probabilities of IIExp, IExpI, IExpExp, ExpII, ExpIExp, ExpExpI, and
947 ExpExpExp triplets (W_{IIExp}, W_{IExpI}, $W_{IExpExp}$, W_{ExpII}, $W_{ExpIExp}$, $W_{ExpExpI}$, and $W_{ExpExpExp}$) are
948 decreasing. In table A-2 such triplets are identified with an arrow following their occurrence
949 probability. To distribute these “disappearing” layer triplets among newly formed ones, the
950 R = 1 Reichweit parameter implies that the transition probability from one layer pair to
951 another does not depend on the preceding or following layer. As an illustration, one may
952 consider the transformation of the 0.1481 IIExp triplets present in I-Exp from sample C. As
953 IExp pairs may be transformed to II, IExp, and ICh pairs (table A-3A) IIExp triplets are
954 transformed to III, IIExp, and IICh triplets (0.0063 = 0.1481 × 0.0094 ÷ 0.2211, 0.1204 =

0.1481 × 0.1798 ÷ 0.2211, and 0.0214 = 0.1481 × 0.0319 ÷ 0.2211, respectively). In this case, the initial layer pair (II) is not modified during transformation from I-Exp in sample C to intermediate phase I. If both the initial and final layer pairs of a triplet are modified (such as for IExpI triplets from sample C), the two modifications have to be considered separately. Transformation of the first layer pair (IExp) leads to the formation of III, IExpI, and IChI triplets, whereas that of the second layer pair (ExpI) leads to III, IExpI, and IExpCh triplets. Relative proportions of the newly formed layer triplets are calculated as described above (0.0031 = 0.1481 × 0.0094 ÷ (0.2211 + 0.2211), 0.0602 = 0.1481 × 0.1798 ÷ (0.2211 + 0.2211), 0.0214 = 0.1481 × 0.0319 ÷ (0.2211 + 0.2211), 0.0032 = 0.1481 × 0.0095 ÷ (0.2211 + 0.2211), et cetera). These values are reported in table A-3B for all layer triplets and for the different transitions. They can be summed up to calculate theoretical occurrence probabilities for all layer triplets in phase I, phase II, and in the I-Exp-Ch from sample D that are reported in the W_{Cal} columns of table A-2. These values are very similar to those calculated from the XRD structure models determined for I-Exp from sample C and for I-Exp-Ch from sample D, and hypothesized for intermediate phases I and II. Following the transition from I-Exp (sample C) to phase I, differences between W_{Cal} and W_{XRD} are maximum for ExpIExp (0.0115), ChExpI (-0.0080), IExpExp (0.0074), and ExpExpI (0.0069) triplets. For the phase I to phase II transition, these differences are most substantial for ExpIExp (0.0085) and ExpExpI (0.0061) triplets. For the transition from phase II to I-Exp-Ch (sample D), only IChCh and ChChI layer triplets present non-negligible differences between the W_{Cal} and W_{XRD} (-0.0079, and -0.0065, respectively). Overall, the observed agreement between calculated W_{ijk} values and those derived from structure models is excellent and supports the hypothesized solid-state reaction mechanism as it is strongly influenced by the choice of junction probability parameters. In particular, if the $P_{SS} = W_S$ is not maintained for intermediate phases, calculated W_{ijk} values differ significantly from those derived from

980 structure models. However, I-Exp-Ch structure models hypothesized for intermediate phases I
981 and II and layer pair transitions are to be considered only as an approximation to the actual
982 mechanism of I-Exp-Ch formation at the expense of I-Exp.

FIGURE CAPTIONS

Fig. A-1. Experimental XRD patterns obtained from Carter well samples selected as being representative of the complete smectite-to-illite diagenetic transition. Sampling depths are 2170 (A), 3660 (B), 4000 (C), 4640 (D), 5010 (E), and 5180 m (F). Data collected on air-dried samples at 40% relative humidity. Patterns as in figure 1.

Fig. A-2. Elementary contributions to the intensity diffracted by sample B (3660 m). Patterns as for figure 5. The structural parameters for the optimal models are given in table 4A. **A**. Air-dried sample. **B**. EG solvated sample.

Fig. A-3. Elementary contributions to the intensity diffracted by sample E (5010 m). Patterns as for figure 5. The structural parameters for the optimal models are given in table 4C. **A**. Air-dried sample. **B**. EG solvated sample.

Fig. A-4. Sensitivity of calculated XRD patterns to structural parameters. Patterns as for figure 5. **A**. Sample E – 5010 m Ca-saturated air-dried. Elementary contribution of the optimum I-Exp-Ch (table 4C). **B**. Sample E – 5010 m Ca-saturated air-dried. 14.0 Å Ch layers (with 3.0 Mg and 6.0 OH per half unit-cell in their interlayers) of the optimum I-Exp-Ch are replaced by 14.0 Å Exp layers (with 0.25 Mg and 2.0 OH per half unit-cell in their interlayers).

Table A-1A. Single-phase segregated I-Exp model. Relative abundance of the different layer pairs (W_{ij} parameters) calculated for the segregated I-Exp from sample A.

A-AD	I 9.98 Å	Exp1 15.00 Å	Exp2 12.50 Å	Exp3 14.00 Å
I 9.98 Å	0.270	0.060	0.060	0.060
Exp1 15.00 Å	0.060	0.150	0.050	0.040
Exp2 12.50 Å	0.060	0.050	0.040	0.000
Exp3 14.00 Å	0.060	0.040	0.000	0.000

A-EG	I 9.98 Å	Exp 16.76 Å
I 9.98 Å	0.270	0.180
Exp 16.76 Å	0.180	0.370

Note: The W_{ij} matrices obtained for AD and EG states are equivalent if $Exp_{EG} = Exp1_{AD} + Exp2_{AD} + Exp3_{AD}$.

Table A-1B. Single-phase segregated I-Exp model. Relative abundance of the different layer pairs (W_{ij} parameters) calculated for the segregated I-Exp from sample B.

B-AD	I 9.98 Å	Exp1 15.00 Å	Exp2 12.50 Å
I 9.98 Å	0.465	0.116	0.069
Exp1 15.00 Å	0.109	0.074	0.027
Exp2 12.50 Å	0.075	0.021	0.044

B-EG	I 9.98 Å	Exp1 16.76 Å	Exp2 14.00 Å
I 9.98 Å	0.465	0.140	0.044
Exp1 16.76 Å	0.140	0.130	0.000
Exp2 14.00 Å	0.044	0.000	0.036

B	I	Exp1	Exp’	Exp2
I	0.465	0.116	0.025	0.044
Exp1	0.109	0.074	0.027	0.000
Exp’	0.031	0.021	0.008	0.000
Exp2	0.044	0.000	0.000	0.036

Note: The W_{ij} matrices obtained for AD and EG states are equivalent if Exp layers from the present table are combined as follows: $Exp1_{AD}$ = Exp1, $Exp2_{AD}$ = Exp’ + Exp2, $Exp1_{EG}$ = Exp1 + Exp’, and $Exp2_{EG}$ = Exp2.

Table A-1C. Single-phase segregated I-Exp model. Relative abundance of the different layer pairs (W_{ij} parameters) calculated for the segregated I-Exp from sample C.

C-AD	I 9.98 Å	Exp1 15.00 Å	Exp2 12.50 Å
I 9.98 Å	0.445	0.090	0.116
Exp1 14.90 Å	0.090	0.023	0.038
Exp2 12.50 Å	0.116	0.048	0.036

C-EG	I 9.98 Å	Exp1 16.76 Å	Exp2 14.00 Å
I 9.98 Å	0.444	0.162	0.044
Exp1 16.76 Å	0.162	0.108	0.000
Exp2 14.00 Å	0.044	0.000	0.036

C	I	Exp1	Exp’	Exp2
I	0.445	0.090	0.072	0.044
Exp1	0.090	0.023	0.038	0.000
Exp’	0.072	0.048	0.000	0.000
Exp2	0.044	0.000	0.000	0.036

Note: The W_{ij} matrices obtained for AD and EG states are equivalent if Exp layers from the present table are combined as follows: $Exp1_{AD}$ = Exp1, $Exp2_{AD}$ = Exp’ + Exp2, $Exp1_{EG}$ = Exp1 + Exp’, and $Exp2_{EG}$ = Exp2.

Table A-2. Relative abundance of layers, layer pairs and triplets determined for the hypothesized solid-state transformation transition between the I-Exp phase from sample C and the I-Exp-Ch phase from sample D.

	Samples							
Layer Sequence	Sample C		Inter. phase I		Inter. phase II		Sample D	
	W_{XRD}		W_{Cal}	W_{XRD}	W_{Cal}	W_{XRD}	W_{Cal}	W_{XRD}
I	0.67		0.68	0.68	0.69	0.69	0.70	0.70
Exp	0.33	→	0.27	0.27 →	0.21	0.21 →	0.15	0.15
Ch	0.00		0.05	0.05	0.10	0.10	0.15	0.15
II	0.4489		0.4684	0.4684	0.4879	0.4878	0.5072	0.5072
IExp	0.2211	→	0.1798	0.1798 →	0.1413	0.1413 →	0.1050	0.1050
ICh	0.0000		0.0319	0.0319	0.0609	0.0609	0.0878	0.0878
ExpI	0.2211	→	0.1836	0.1836 →	0.1449	0.1449 →	0.1050	0.1050
ExpExp	0.1089	→	0.0729	0.0729 →	0.0441	0.0441 →	0.0225	0.0225
ExpCh	0.0000		0.0135	0.0135	0.0210	0.0210	0.0225	0.0225
ChI	0.000		0.0280	0.0280	0.0573	0.0573	0.0878	0.0878
ChExp	0.000		0.0173	0.0173	0.0246	0.0246 →	0.0225	0.0225
ChCh	0.000		0.0046	0.0046	0.0181	0.0181	0.0397	0.0398
III	0.3008		0.3200	0.3226	0.3424	0.3449	0.3647	0.3676
IIExp	0.1481	→	0.1241	0.1238 →	0.1007	0.0999 →	0.0768	0.0761
IICh	0.0000		0.0214	0.0219	0.0419	0.0430	0.0621	0.0636
IExpI	0.1481	→	0.1217	0.1223 →	0.0958	0.0975 →	0.0716	0.0735
IExpExp	0.0730	→	0.0559	0.0485 →	0.0356	0.0297 →	0.0204	0.0158
IExpC	0.0000		0.0030	0.0090	0.0104	0.0141	0.0143	0.0158
IChI	0.0000		0.0201	0.0179	0.0374	0.0349	0.0545	0.0513
IChExp	0.0000		0.0109	0.0110	0.0180	0.0150 →	0.0180	0.0132
IChCh	0.0000		0.0010	0.0030	0.0056	0.0110	0.0154	0.0233
ExpII	0.1481	→	0.1267	0.1265 →	0.1032	0.1024 →	0.0768	0.0761
ExpIExp	0.0730	→	0.0600	0.0485 →	0.0382	0.0297 →	0.0218	0.0158
ExpICh	0.0000		0.0053	0.0086	0.0125	0.0128	0.0156	0.0132
ExpExpI	0.0730	→	0.0567	0.0496 →	0.0365	0.0304 →	0.0205	0.0158
ExpExpExp	0.0359	→	0.0240	0.0197 →	0.0120	0.0093 →	0.0048	0.0034
ExpExpCh	0.0000		0.0022	0.0036	0.0046	0.0044 →	0.0024	0.0034
ExpChI	0.0000		0.0091	0.0076	0.0147	0.0120	0.0169	0.0132
ExpChExp	0.0000		0.0051	0.0047	0.0067	0.0052 →	0.0050	0.0034
ExpChCh	0.0000		0.0008	0.0013	0.0031	0.0038	0.0064	0.0060
ChII	0.0000		0.0188	0.0193	0.0395	0.0405	0.0630	0.0636
ChIExp	0.0000		0.0046	0.0074	0.0113	0.0117	0.0149	0.0132
ChICh	0.0000		0.0000	0.0013	0.0013	0.0051	0.0051	0.0110
ChExpI	0.0000		0.0038	0.0118	0.0132	0.0170 →	0.0130	0.0158
ChExpExp	0.0000		0.0029	0.0047	0.0057	0.0052 →	0.0034	0.0034
ChExpCh	0.0000		0.0000	0.0009	0.0009	0.0025	0.0026	0.0034
ChChI	0.0000		0.0010	0.0026	0.0052	0.0104	0.0168	0.0233
ChChExp	0.0000		0.0008	0.0016	0.0034	0.0045	0.0068	0.0060
ChChCh	0.0000		0.0000	0.0004	0.0004	0.0033	0.0068	0.0105

Note: W_{XRD} values are deduced directly from the structure model determined from I-Exp in sample C and for I-Exp-Ch in sample D. For the theoretical phase I and II, W_{XRD} values are deduced from the hypothesized structure models intermediate between the two end-members (see text for details). W_{Cal} values are calculated assuming the redistribution of layers, layer pairs and triplets whose relative proportion is decreasing from one step to the next one. These layers, layer pairs and triplets are indicated by arrows in the present table. Redistribution of these layers, layer pairs and triplets is described in table A-3.

Table A-3A. Redistribution of layer pairs whose relative proportion is decreasing from one step to the next one during the hypothesized solid-state transformation transition between the I-Exp phase in sample C and the I-Exp-Ch phase in sample D.

I-Exp in sample C		⇨ Phase I	
0.2211	IExp	II	0.0094
		IExp	0.1798
		ICh	0.0319
0.2211	ExpI	II	0.0095
		ExpI	0.1836
		ChI	0.0280
0.1089	ExpExp	II	0.0006
		ExpCh	0.0135
		ExpExp	0.0729
		ChExp	0.0173
		ChCh	0.0046

Note: Layer pairs whose proportion is stable or increasing during any of the three steps are not reported in the present table. Their relative abundances, reported in table A-2, are calculated as the sum of their relative abundance in the previous reaction step and of the present redistribution.

Phase I		⇨ Phase II	
0.1798	IExp	II	0.0095
		IExp	0.1413
		ICh	0.0290
0.1836	ExpI	II	0.0095
		ExpI	0.1449
		ChI	0.0292
0.0729	ExpExp	II	0.0005
		ExpCh	0.0075
		ExpExp	0.0441
		ChExp	0.0073
		ChCh	0.0135

Phase II		⇨	I-Exp-Ch in sample D	
0.1413	IExp		II	0.0094
			IExp	0.1050
			ICh	0.0269
0.1449	ExpI		II	0.0094
			ExpI	0.1050
			ChI	0.0305
0.0441	ExpExp		II	0.0006
			ExpCh	0.0015
			ExpExp	0.0225
			ChCh	0.0195
0.0246	ChExp		ChExp	0.0225
			ChCh	0.0021

Table A-3B. Redistribution of layer triplets whose relative proportion is decreasing from one step to the next one during the hypothesized solid-state transformation transition between the I-Exp phase in sample C and the I-Exp-Ch phase in sample D.

I-Exp in sample C		⇨	Phase I	
0.1481	IIExp		III	0.0063
			IIExp	0.1204
			IICh	0.0214
0.1481	IExpI		III	0.0031
			IExpI	0.0602
			IChI	0.0107
			III	0.0032
			IExpI	0.0615
			IChI	0.0094
0.0730	IExpExp		IIExp	0.0021
			IExpExp	0.0398
			IChExp	0.0071
			III	0.0001
			IExpCh	0.0030
			IExpExp	0.0161
			IChExp	0.0038
			IChCh	0.0010
0.1481	ExpII		III	0.0064
			ExpII	0.1230
			ChII	0.0188
0.0730	ExpIExp		IIExp	0.0016
			ExpIExp	0.0303
			ChIExp	0.0046
			ExpII	0.0016
			ExpIExp	0.0297
			ExpICh	0.0053
0.0730	ExpExpI		III	0.0001
			ExpChI	0.0029
			ExpExpI	0.0161
			ChExpI	0.0038
			ChChI	0.0010
			ExpII	0.0021
			ExpExpI	0.0406
			ExpChI	0.0062
0.0359	ExpExpExp		ExpChExp	0.0022
			ExpExpExp	0.0120
			ChExpExp	0.0029
			ChChExp	0.0008
			ExpExpCh	0.0022
			ExpExpExp	0.0120
			ExpChExp	0.0029

	ExpChCh	0.0008

Note: The redistribution of layer triplets among newly formed ones is done assuming that the transition probability from one layer pair to another does not depend on the preceding or following layer as R = 1 (see text for details). Layer triplets whose proportion is stable or increasing during any of the three steps are not reported in the present table. Their relative abundances, reported in table A-2, are calculated as the sum of their relative abundance in the previous reaction step and of the present redistribution.

Table A-3B continued

Phase I		Phase II	
0.1241	IIExp	III	0.0066
		IIExp	0.0975
		IICh	0.0200
0.1217	IExpI	III	0.0032
		IExpI	0.0473
		IChI	0.0097
		III	0.0032
		IExpI	0.0485
		IChI	0.0098
0.0485	IExpExp	IIExp	0.0018
		IExpExp	0.0271
		IChExp	0.0056
		III	0.0001
		IExpCh	0.0014
		IExpExp	0.0085
		IChExp	0.0014
		IChCh	0.0026
0.1267	ExpII	III	0.0066
		ExpII	0.1000
		ChII	0.0202
0.0485	ExpIExp	IIExp	0.0013
		ExpIExp	0.0189
		ChIExp	0.0039
		ExpII	0.0013
		ExpIExp	0.0193
		ExpICh	0.0039
0.0496	ExpExpI	III	0.0001
		ExpChI	0.0015
		ExpExpI	0.0085
		ChExpI	0.0014
		ChChI	0.0026
		ExpII	0.0018
		ExpExpI	0.0280
		ExpChI	0.0056
0.0197	ExpExpExp	IIExp	0.0001
		ExpChExp	0.0010
		ExpExpExp	0.0060
		ChExpExp	0.0010
		ChChExp	0.0018
		ExpII	0.0001
		ExpExpCh	0.0010
		ExpExpExp	0.0060
		ExpChExp	0.0010
		ExpChCh	0.0018

Table A-3B continued

Phase II		⇨	I-Exp-Ch in sample D	
0.0999	IIExp		III	0.0066
			IIExp	0.0742
			IICh	0.0190
0.0975	IExpI		III	0.0032
			IExpI	0.0358
			IChI	0.0092
			III	0.0032
			IExpI	0.0358
			IChI	0.0104
0.0297	IExpExp		IIExp	0.0015
			IExpExp	0.0168
			IChExp	0.0043
			III	0.0001
			IExpCh	0.0002
			IExpExp	0.0036
			IChCh	0.0031
0.0150	IChExp		IChExp	0.0137
			IChCh	0.0013
0.1024	ExpII		III	0.0066
			ExpII	0.0742
			ChII	0.0216
0.0297	ExpIExp		IIExp	0.0010
			ExpIExp	0.0109
			ChIExp	0.0032
			ExpII	0.0010
			ExpIExp	0.0109
			ExpICh	0.0028
0.0304	ExpExpI		III	0.0001
			ExpExpI	0.0036
			ChExpI	0.0002
			ChChI	0.0031
			ExpII	0.0015
			ExpExpI	0.0169
			ExpChI	0.0049
0.0093	ExpExpExp		IIExp	0.0001
			ExpChExp	0.0002
			ExpExpExp	0.0024
			ChChExp	0.0021
			ExpII	0.0001
			ExpExpCh	0.0002
			ExpExpExp	0.0024
			ExpChCh	0.0021

Table A-3B continued

Phase II		⇨ I-Exp-Ch in sample D	
0.0150	ExpExpCh	IICh	0.0001
		ExpExpCh	0.0022
		ExpChCh	0.0001
		ChChCh	0.0020
0.0052	ExpChExp	ExpChExp	0.0048
		ExpChCh	0.0004
0.0170	ChExpI	ChExpI	0.0023
		ChChI	0.0002
		ChII	0.0009
		ChExpI	0.0105
		ChChI	0.0031
0.0052	ChExpExp	ChExpExp	0.0017
		ChChExp	0.0002
		ChII	0.0000
		ChExpExp	0.0017
		ChExpCh	0.0001
		ChChCh	0.0015

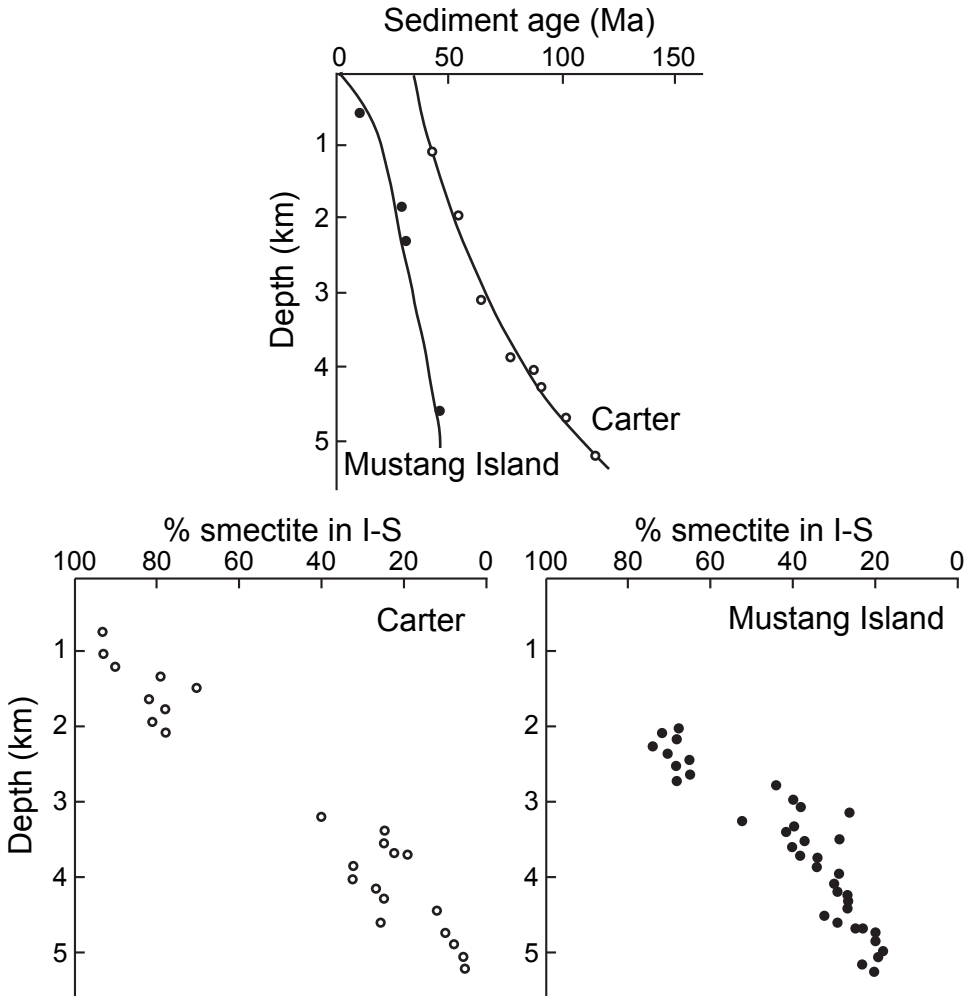

Lanson et al. Fig. 1

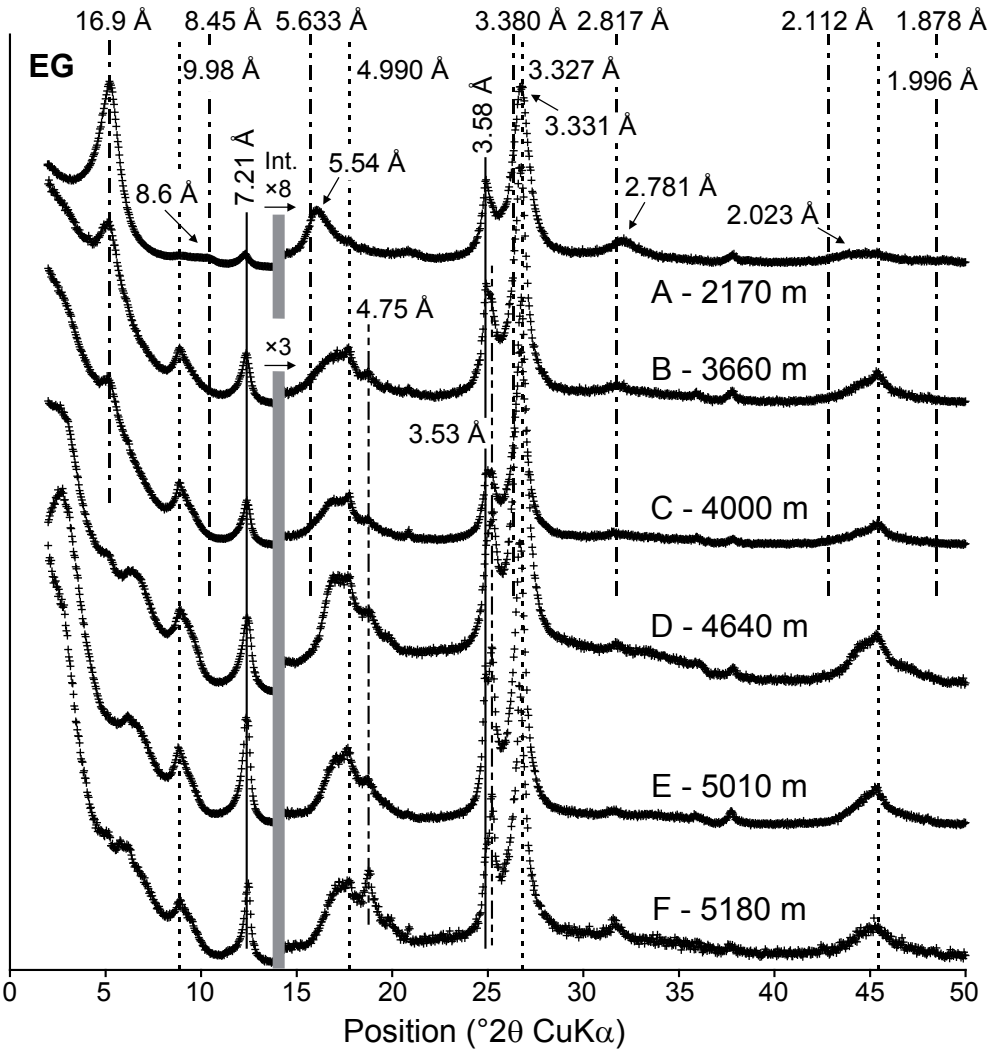

Lanson et al. Fig. 2

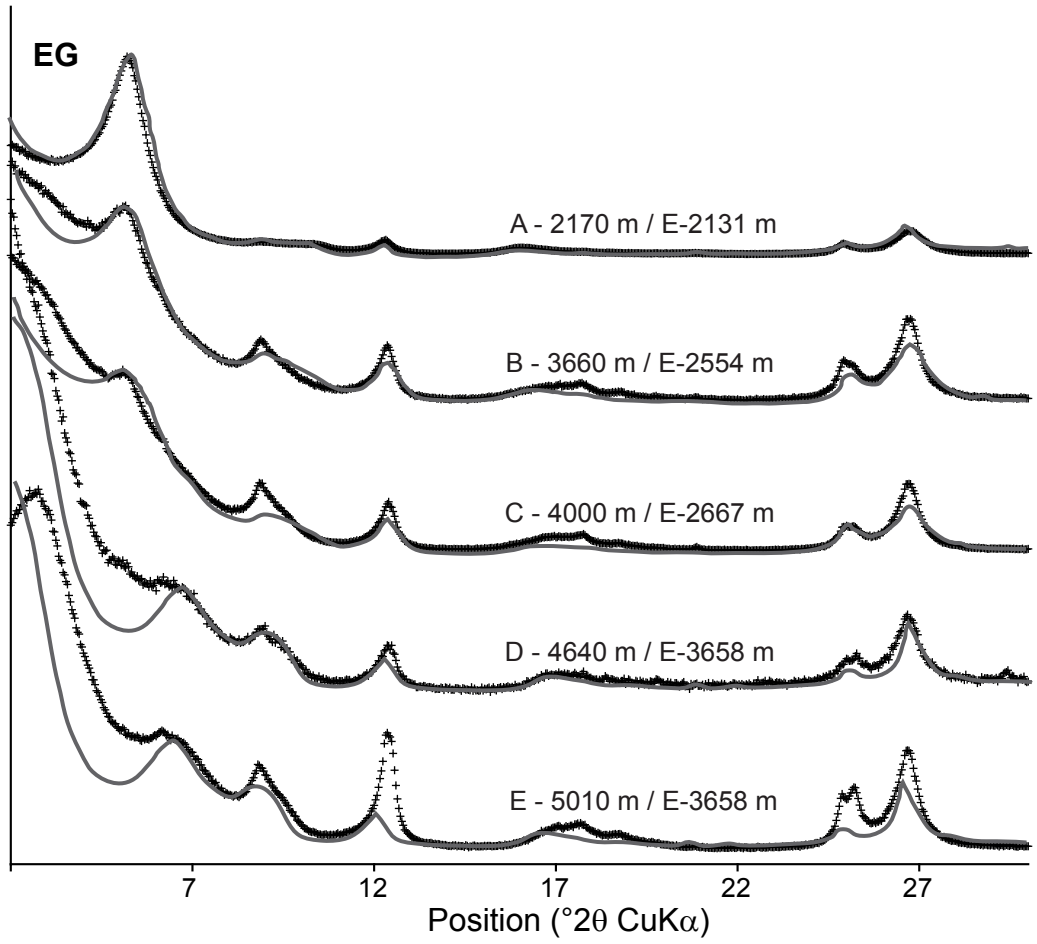

Lanson et al. Fig. 3

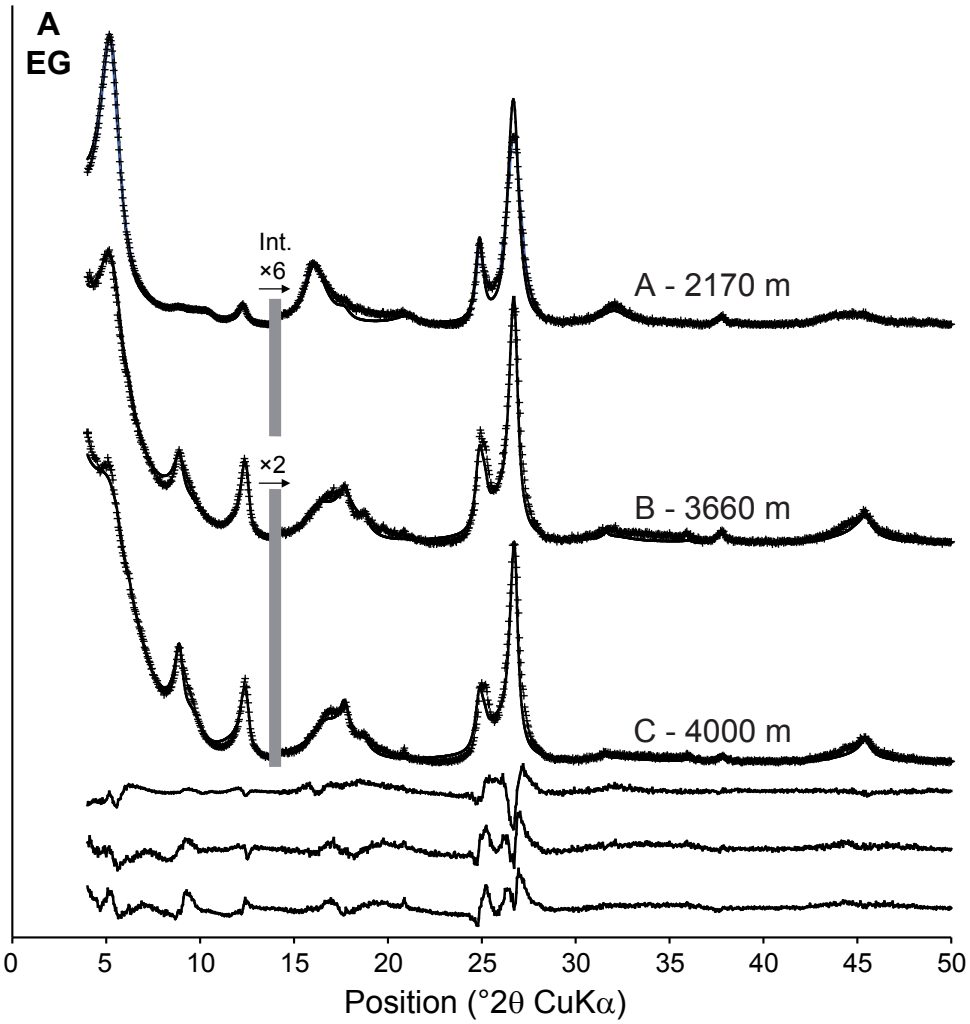

Lanson et al. Fig. 4A

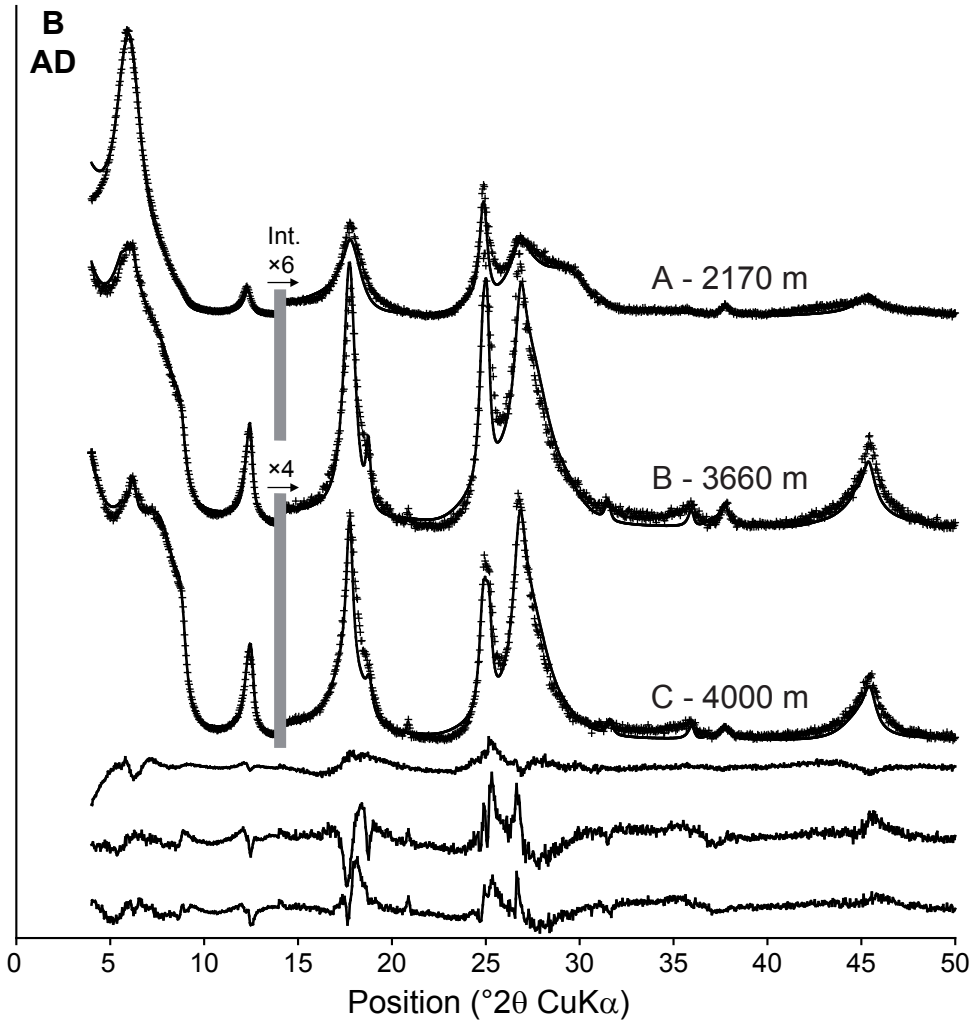

Lanson et al. Fig. 4B

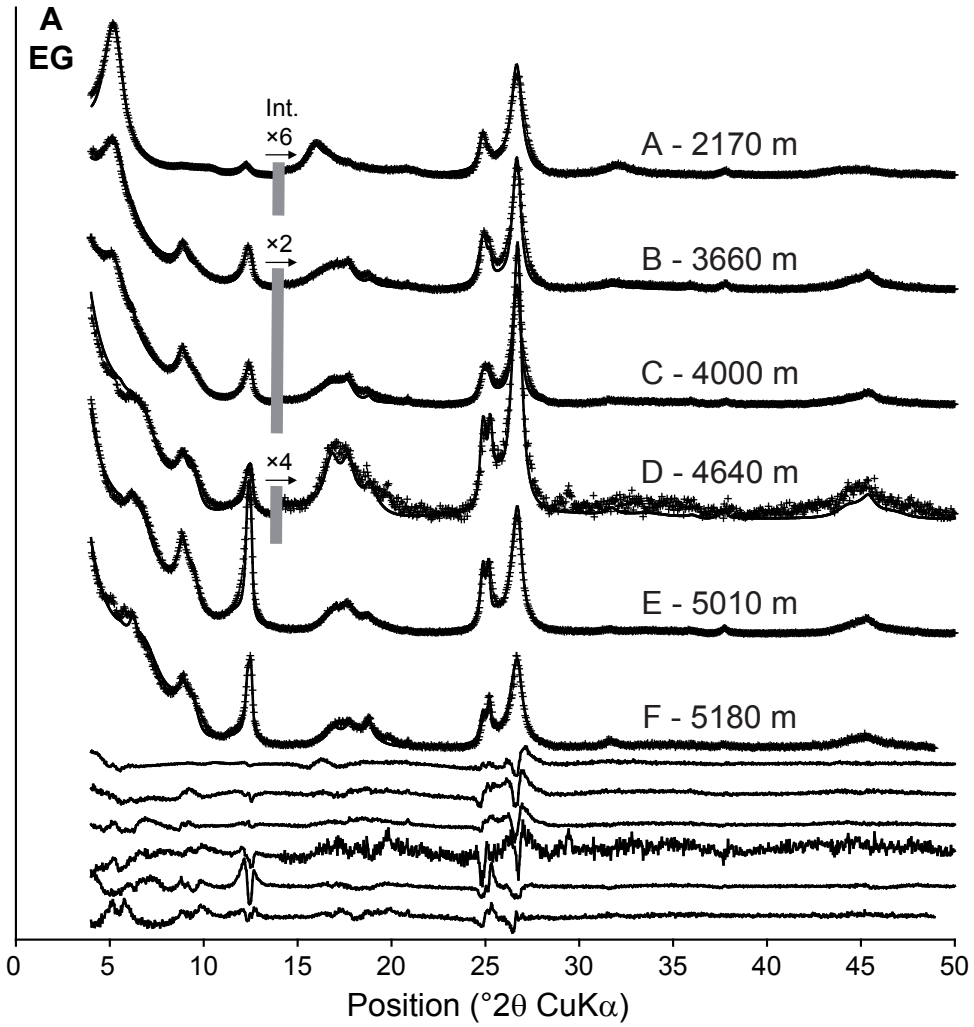

Lanson et al. Fig. 5A

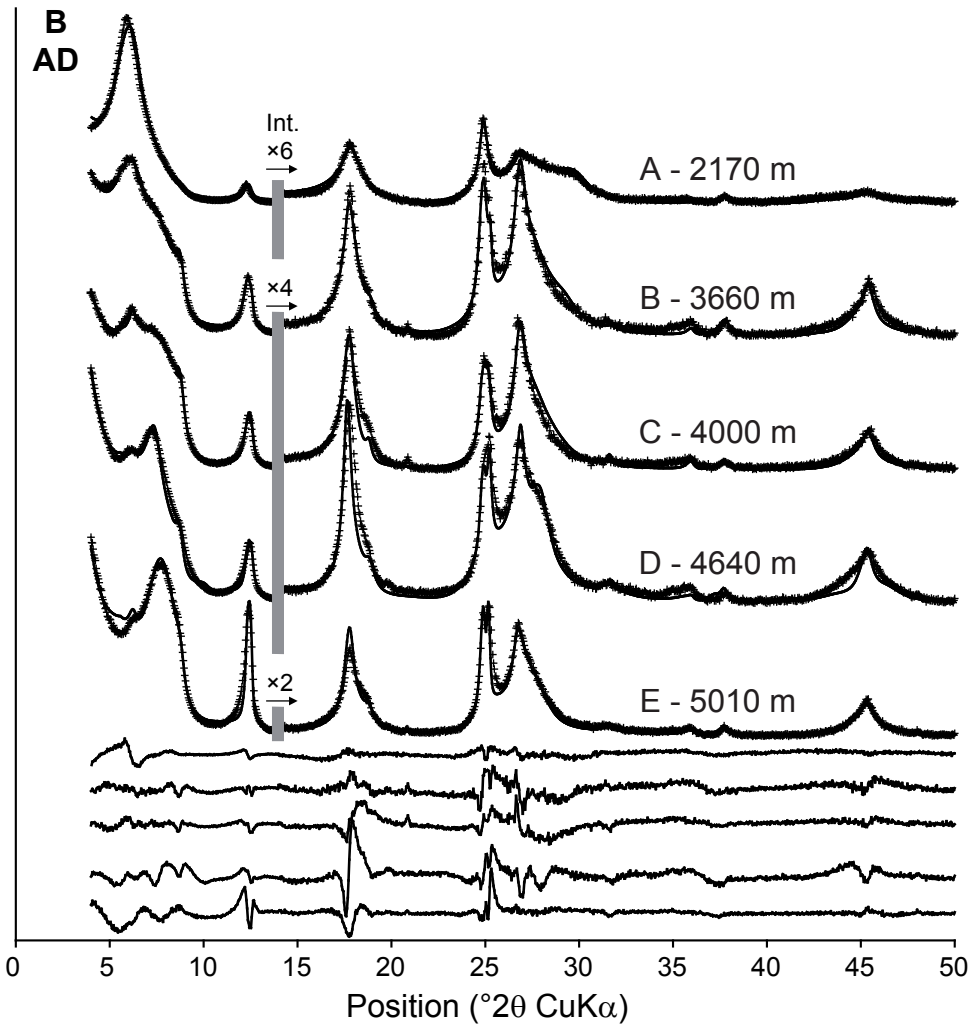

Lanson et al. Fig. 5B

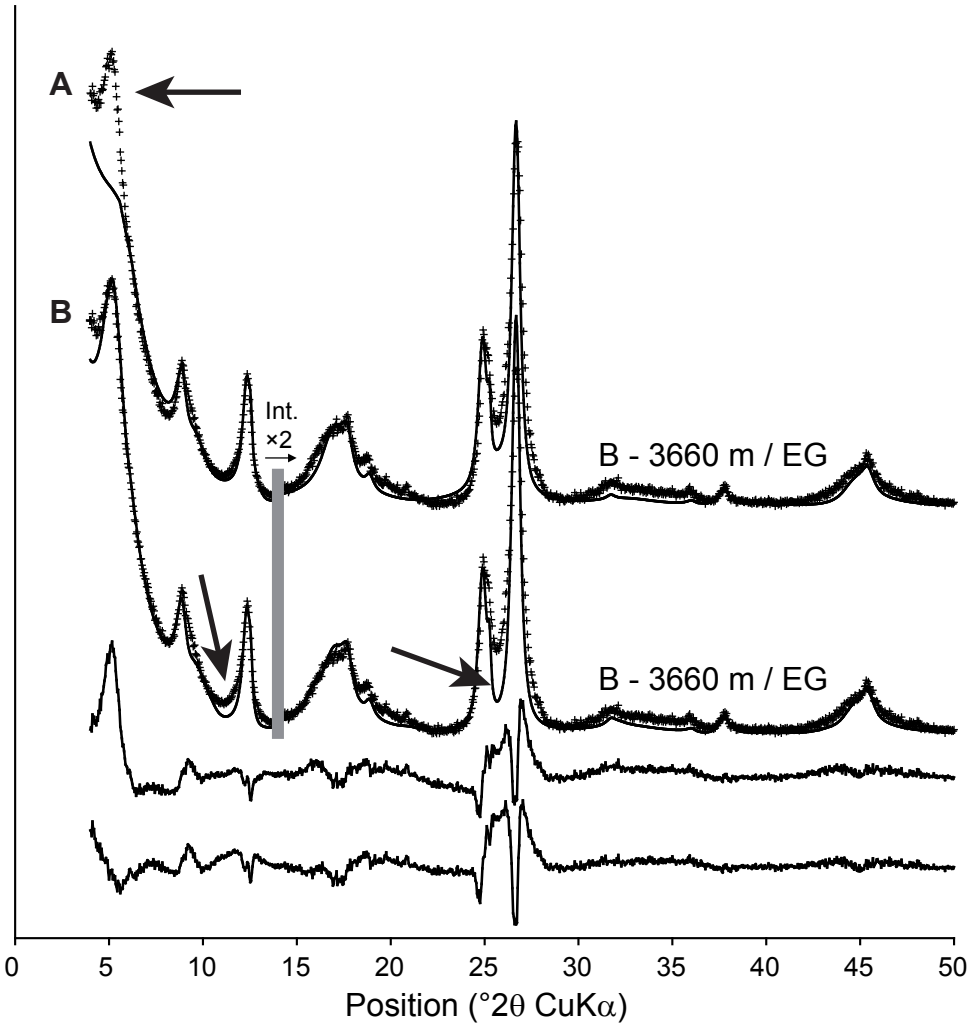

Lanson et al. Fig. 6

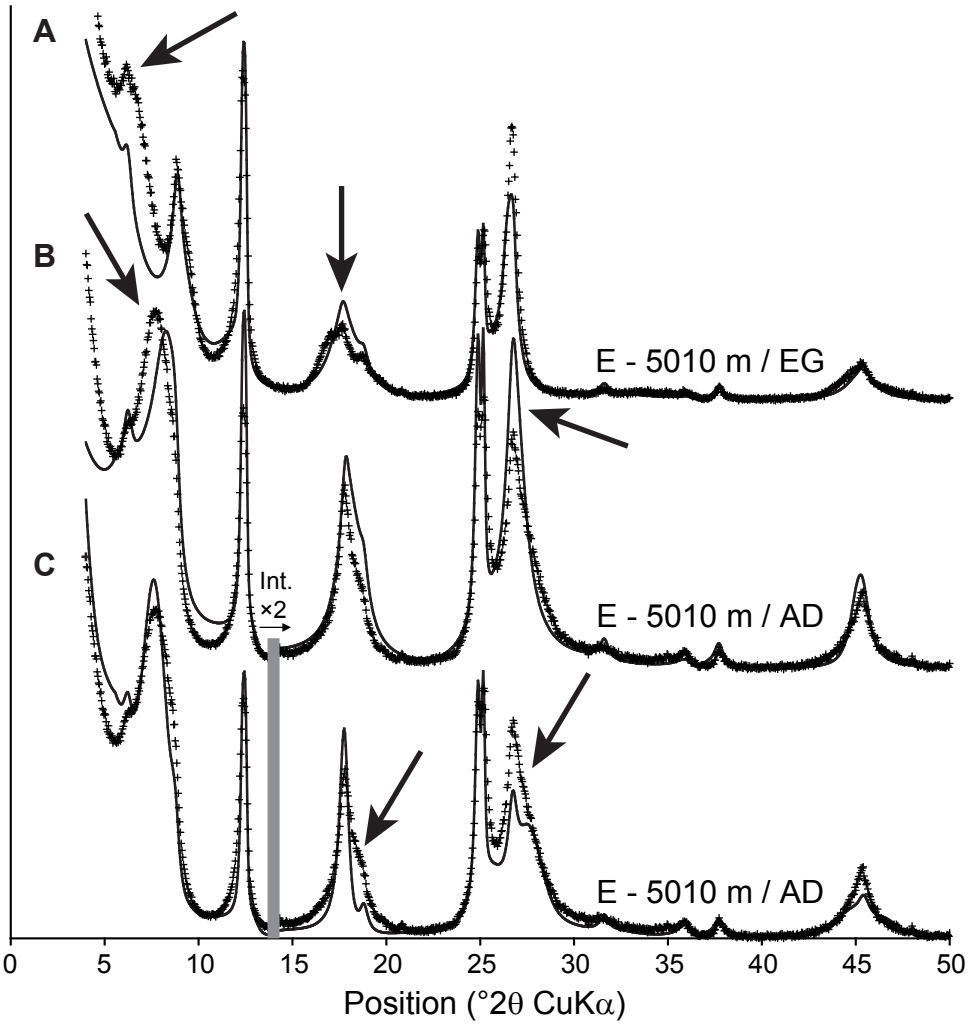

Lanson et al. Fig. 7

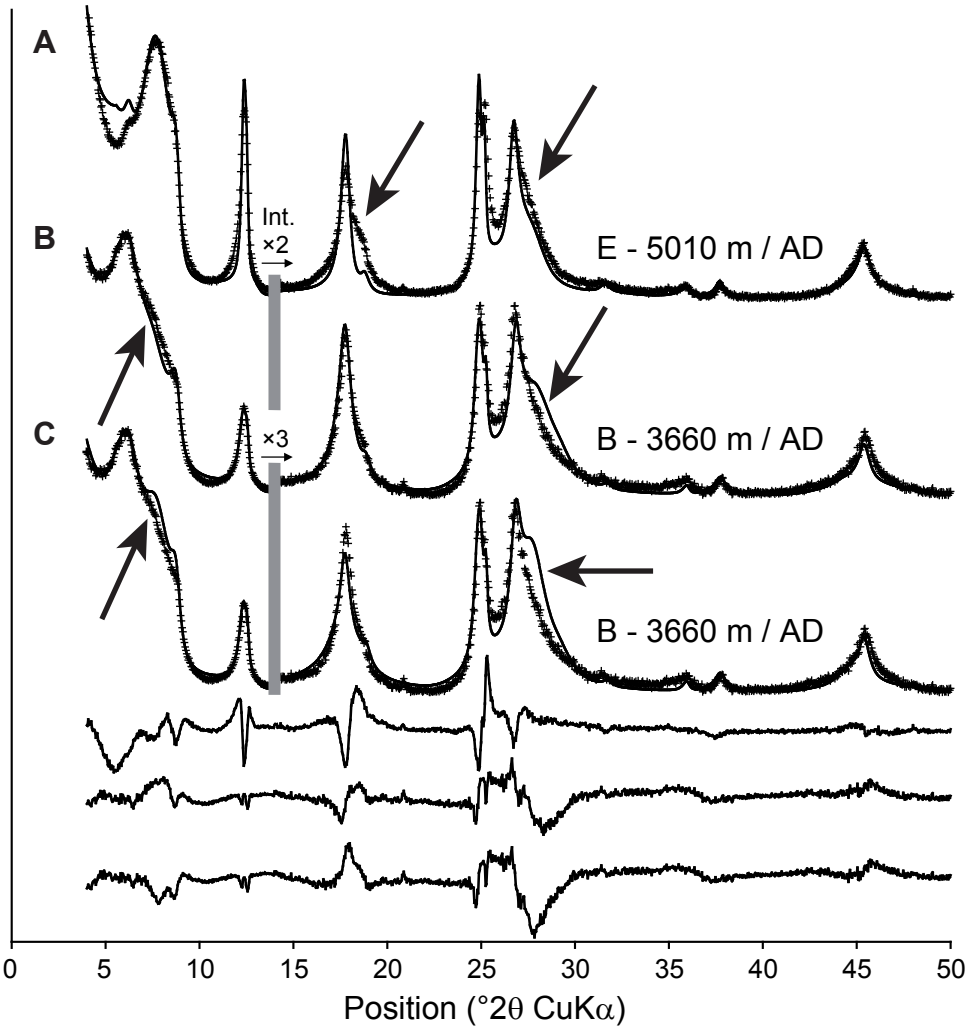

Lanson et al. Fig. 8

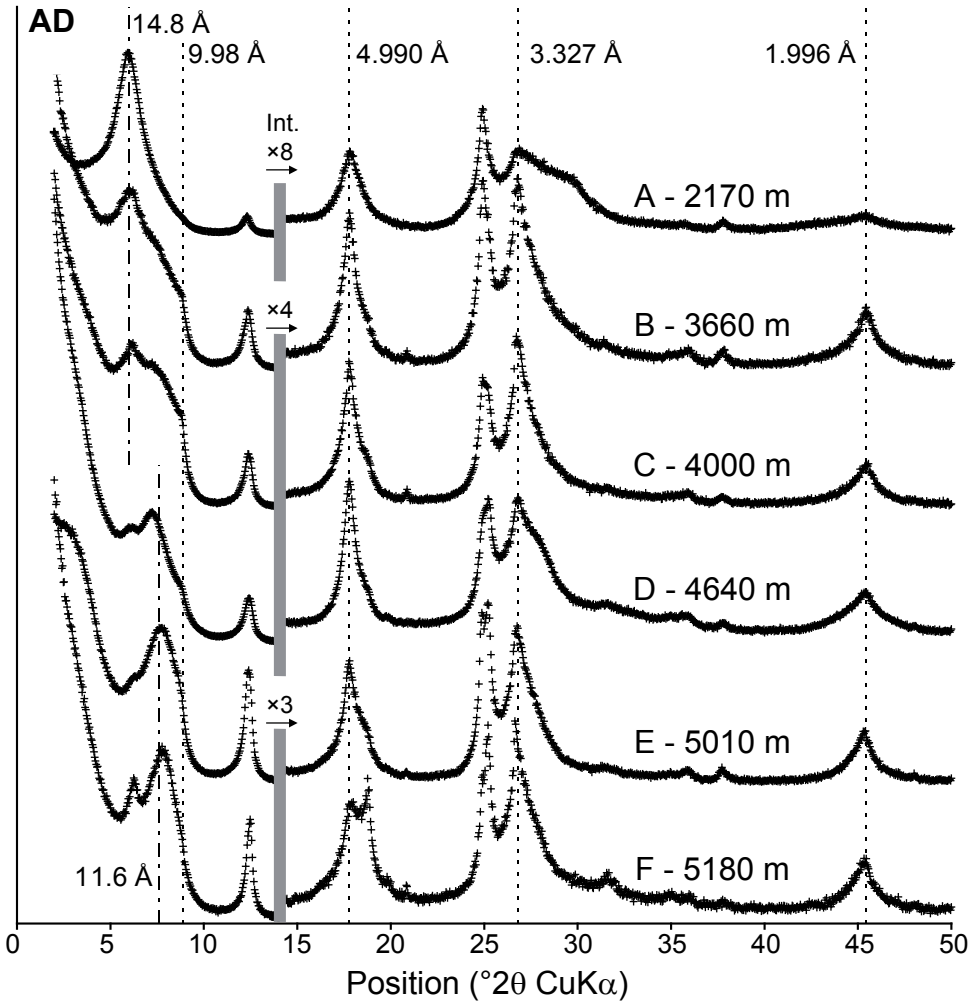

Lanson et al. Fig. A-1

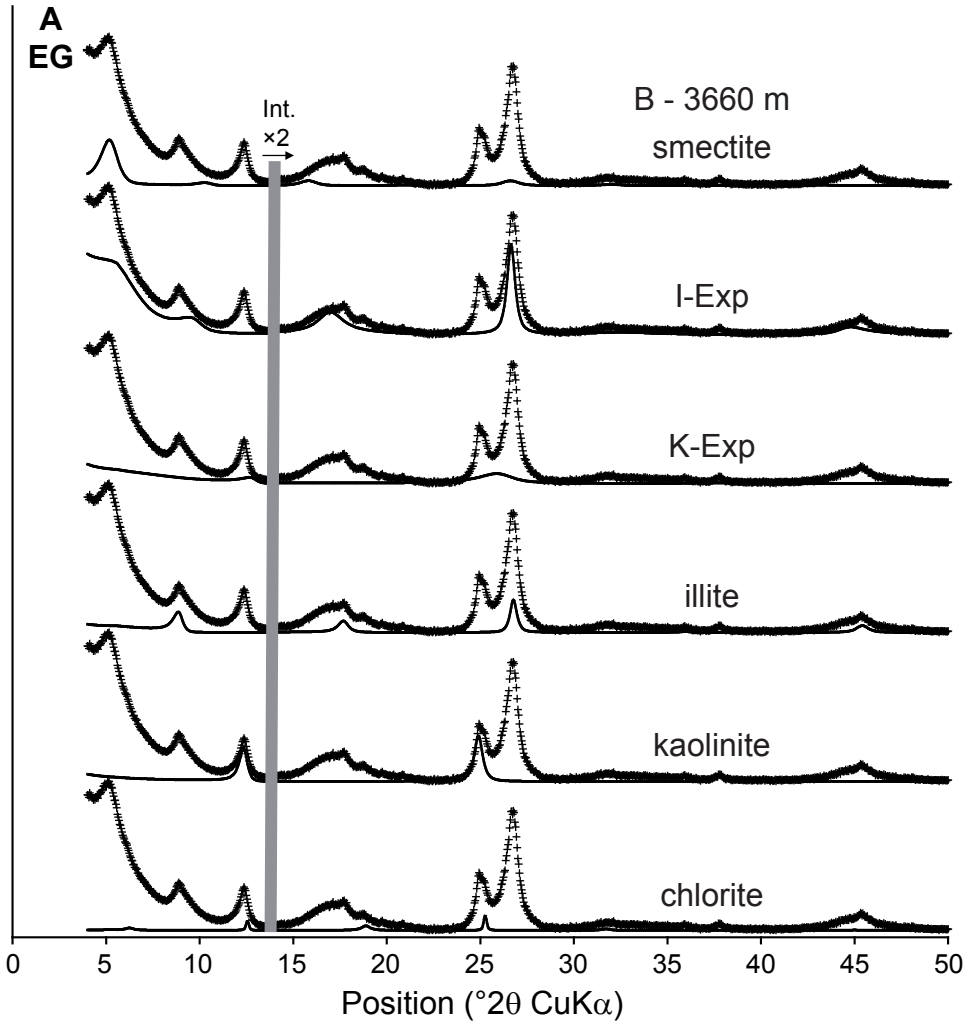

Lanson et al. Fig. A-2A

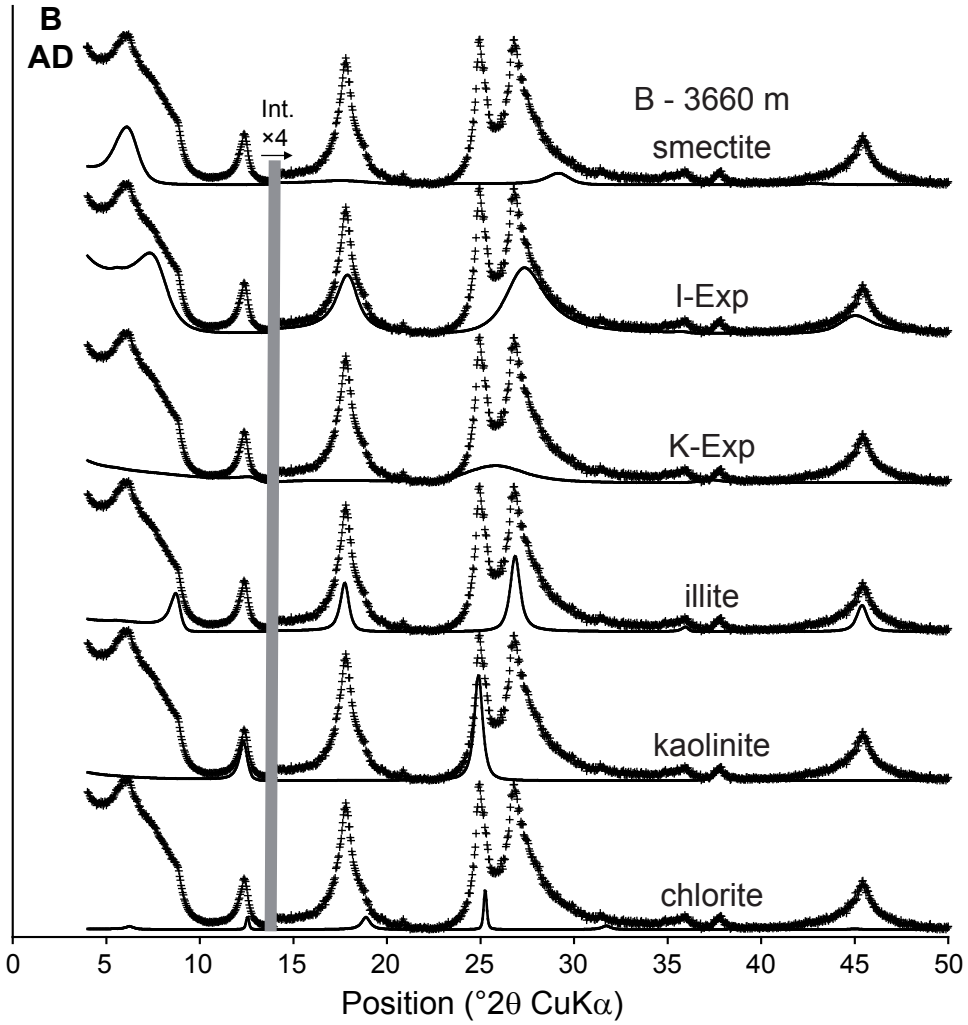

Lanson et al. Fig. A-2B

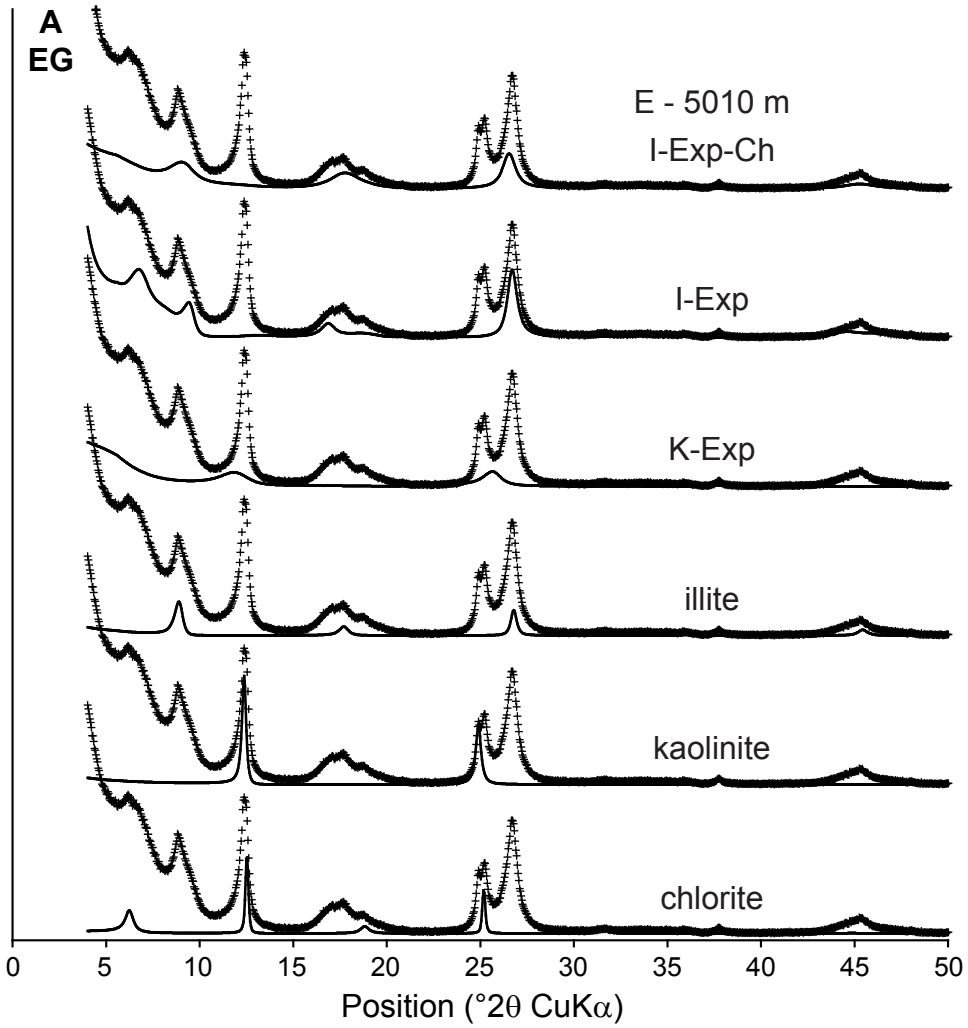

Lanson et al. Fig. A-3A

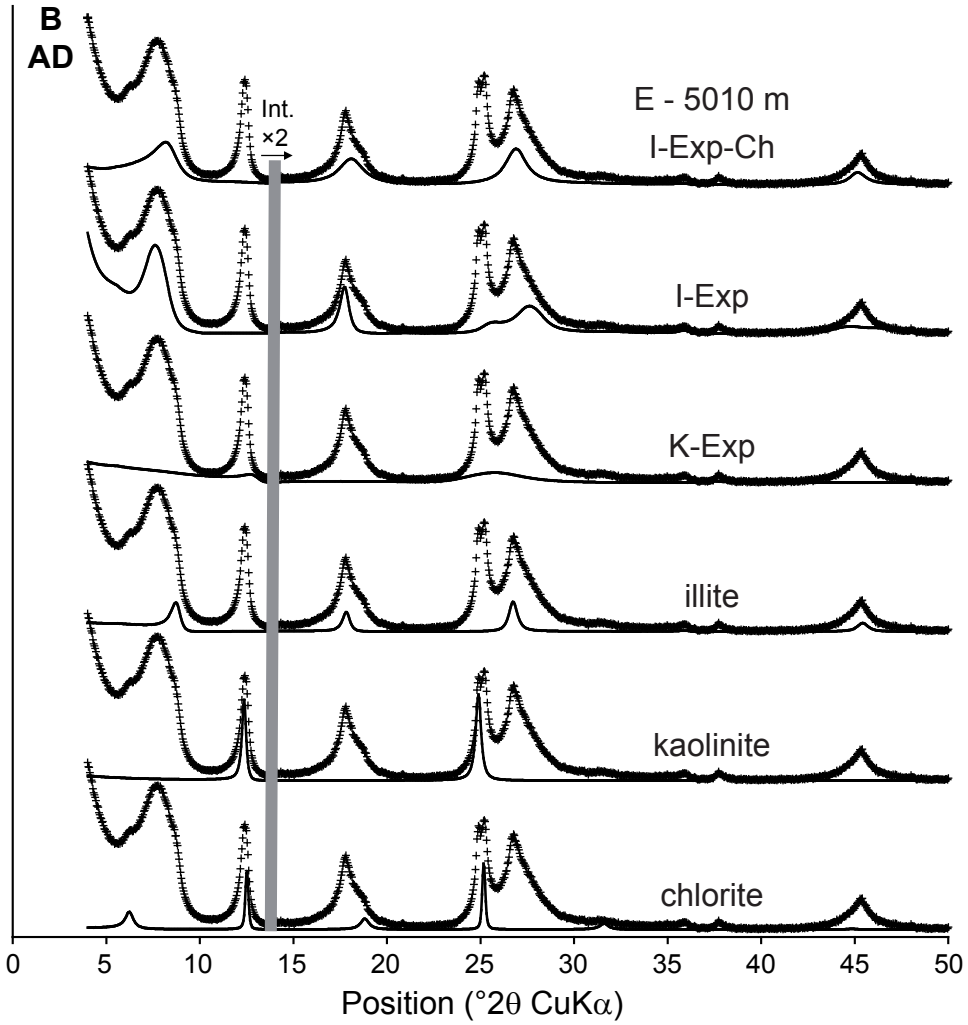

Lanson et al. Fig. A-3B

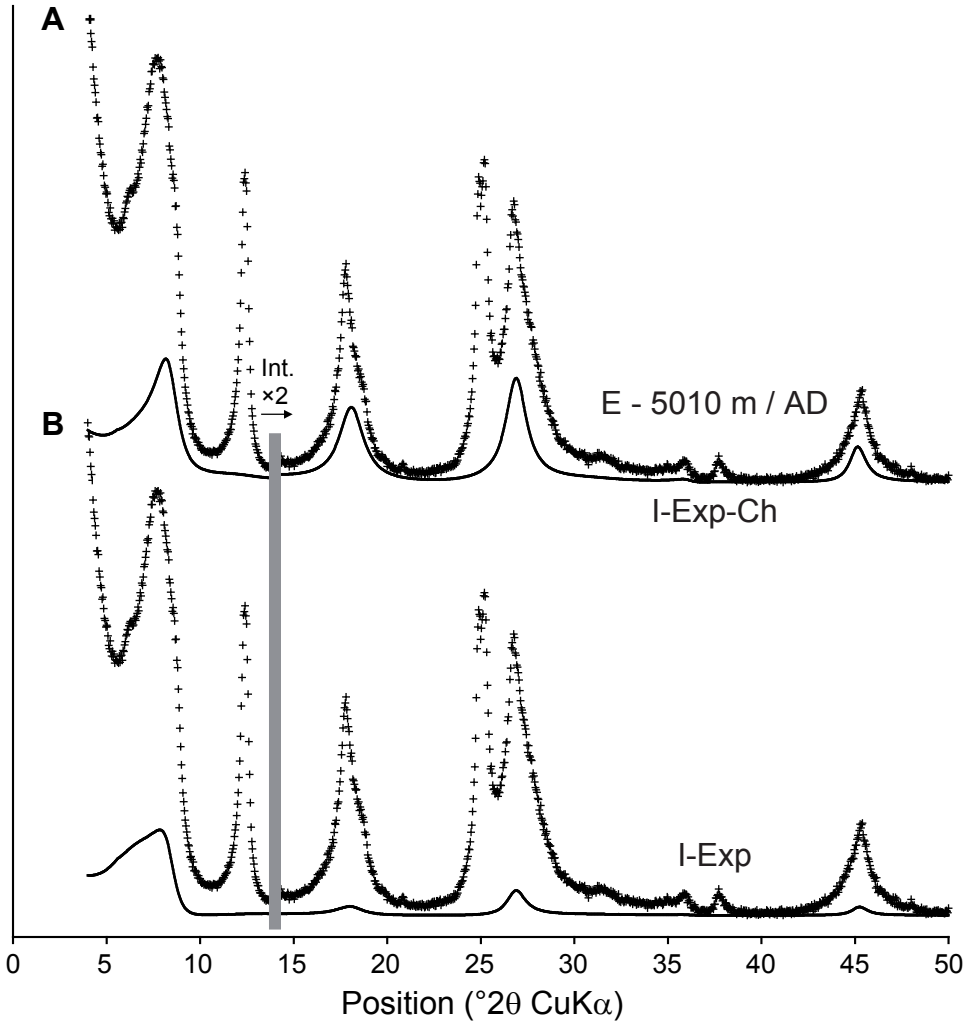

Lanson et al. Fig. A-4